Submitted to ApJ

The History of Cosmological Star Formation: Three Independent Approaches and a Critical Test Using the Extragalactic Background Light

Kentaro Nagamine[1], Jeremiah P. Ostriker[2], Masataka Fukugita[3,4], & Renyue Cen[2]

ABSTRACT

Taking three independent approaches, we investigate the simultaneous constraints set on the cosmic star formation history from various observations, including stellar mass density and extragalactic background light (EBL). We compare results based on: 1) direct observations of past light-cone, 2) a model using local fossil evidence constrained by SDSS observations at $z \sim 0$ (the 'Fossil' model), and 3) theoretical *ab initio* models from three calculations of cosmic star formation history: (a) new $(1024)^3$ Total Variation Diminishing (TVD) cosmological hydrodynamic simulation, (b) analytic expression of Hernquist & Springel based on cosmological Smoothed Particle Hydrodynamics (SPH) simulations, and (c) semi-analytic model of Cole et al. We find good agreement among the three independent approaches up to the order of observational errors, except that all the models predict bolometric EBL of $I_{\rm tot} \simeq 37 - 52$ nW m^{-2} sr^{-1}, which is at the lower edge of the the observational estimate by Hauser & Dwek (2001). We emphasize that the Fossil model that consists of two components — spheroids and disks —, when normalized to the local observations, provides a surprisingly simple but accurate description of the cosmic star formation history and other observable quantities. Our analysis suggests that the consensus global parameters at $z = 0$ are: $\Omega_\star = 0.0023 \pm 0.0004$, $I_{\rm EBL} = 43 \pm 7\,{\rm nW\,m^{-2}\,sr^{-1}}$, $\dot{\rho}_\star = (1.06 \pm 0.22) \times 10^{-2}\,{\rm M_\odot\,yr^{-1}\ Mpc^{-3}}$, $j_{\rm bol} = (3.1 \pm 0.2) \times 10^8\,L_\odot\ {\rm Mpc^{-3}}$.

Subject headings: cosmology: theory — stars: formation — galaxies: formation — galaxies: evolution

[1]University of California, San Diego, Center for Astrophysics and Space Sciences, CA 92093-0424, U.S.A., Email: knagamine@ucsd.edu

[2]Princeton University Observatory, Princeton, NJ 08544, U.S.A.

[3]Institute for Cosmic Ray Research, University of Tokyo, Kashiwa 2778582, Japan

[4]Institute for Advanced Study, Einstein Drive, Princeton NJ, 08540, U.S.A.

1. Introduction

Targets of cosmological investigations during the last decade have largely shifted from the global, geometrical properties of the universe to the detailed contents thereof, particularly the origin and evolution of structure from smooth initial conditions. Of the components added since the decoupling of matter and radiation, stars are the most easily observable feature (emitting the most electromagnetic energy) and of the greatest historical significance. Approximately $6 \pm 2\%$ (e.g., Fukugita & Peebles 2004) of the baryons of the universe have condensed out into stars at the current epoch, and the time history of the process whereby this occurred is the subject of intense study at present. What is not widely realized is that there are three independent approaches by which this study can be pursued:

1. We can use the universe directly as a time-machine: in areas of the sky like the Hubble Deep Field (Williams et al. 1996), attempts have been made to analyze the past light-cone. The rate of transformation of gas into stars is measured as a function of the look-back time or redshift, which produces what has been called the "Madau Diagram" (Madau et al. 1996). There are three major uncertainties involved in this diagram: (1) dust obscuration; (2) relation between emission and star formation rate (SFR), which includes the uncertainty in the initial mass function (IMF); (3) faint-end slope of the luminosity function, especially at high-redshift. All of these three contribute roughly on the same order. Recent observational estimates at $z \gtrsim 4$ suggest a decline in SFR with increasing redshift (Iwata et al. 2003; Bunker et al. 2004; Bouwens et al. 2004; Giavalisco et al. 2004; Ouchi et al. 2004a; Bouwens et al. 2005), but due to uncertainties in dust extinction for ultra-violet (UV) light and the faint-end slope of the luminosity function, the trend does not seem to be inconsistent with being constant at $z > 3$ (See also Figure 2 of Nagamine et al. 2004).

2. The second method predated the direct method outlined above. It uses the fossil record from our own and other galaxies to catalog stars of different ages and to, by an essentially demographic investigation, unravel the history of star formation in the local Universe using the theory of stellar evolution. When direct age estimates are not available, as is the case for external galaxies, color distributions can provide a useful proxy to their history, distinguishing between systems with and without ongoing star formation activity, although there are degeneracies among age, amount of stars formed, metallicity, and IMF. This method was pioneered by Searle, Sargent, & Bagnuolo (1973). Here one makes a simple ansatz for the star formation history — chosen in the quoted paper to be as a simple declining exponential — and an IMF, and then computes, via the standard theories of stellar evolution and stellar atmospheres, the evolving spectral output from the assemblage of stars. They found that one could easily

and plausibly simulate the observed colors of different types of stellar systems. We will update the quantitative input to this theory, leaving the essential basis unchanged, and find that this "Fossil" model fits with uncanny accuracy (given the simplicity of the method) modern observations as obtained by the Sloan Digital Sky Survey (SDSS; York et al. 2000). We will then use SDSS results to determine the parameters of the Fossil model.

3. The third method is to attempt to solve the problem by *ab initio* theory. One takes the initial conditions from the observed cosmic microwave background radiation, adopts a favorite cosmological model, e.g., the standard concordance Λ cold dark matter (CDM) model (Ostriker & Steinhardt 1995; Perlmutter et al. 1998; Riess et al. 1998; Spergel et al. 2003; Tegmark et al. 2004), combines this with the standard physical equations of gravity, hydrodynamics, atomic physics, radiative transfer, *etc.*, and simulates the history of the universe by numerical integration, obtaining as the most important by-product the history of star formation (e.g., Nagamine et al. 2000, 2001b; Ascasibar et al. 2002; Springel & Hernquist 2003b; Nagamine et al. 2004; Nagamine et al. 2006). One could also employ the so-called semi-analytic models of galaxy formation (e.g., Kauffmann et al. 1993; Cole et al. 2000; Somerville et al. 2001), where a dark-matter halo merger-tree, either constructed using the extended Press-Schechter formalism (Bond et al. 1991; Lacey & Cole 1993) or N-body simulations, is supplemented with a set of equations to model transformation of gas into stars within virialized dark matter halos.

If the observational errors are too significant or the theoretical modeling in error, these three independent approaches might not agree with one another when they should. We need to pay particular attention to the errors that are involved in various observations. The quantities at near zero redshift are usually measured without too serious systematic errors. On the other hand, high redshift observations, such as those of star formation rates are subject to large systematic uncertainties from the obscuration and the faint-end slope of luminosity functions. Therefore, we take the attitude that we constrain the three approaches with zero-redshift quantities, while high-redshift observations are used to examine the consistency within allowed errors. We also note that there are some uncertainty such as IMF, but these uncertainties are known and we can see how they propagate to our calculations or even constrain those uncertainties. With understanding those uncertainties, we can conclude that the agreement of the three approaches is in fact good. In addition, there is an independent check of all of these approaches. Each approach predicts two numbers: (1) the local bolometric electromagnetic energy output per unit volume $j_{\rm bol}(z=0)$ [erg sec^{-1} cm^{-3}] and (2) the local energy density $U(z=0)$ [erg cm^{-3}], which is measured as the extragalactic background light (EBL). The first number $j_{\rm bol}(z=0)$ provides a measure of the current star formation rate,

while $U(z = 0)$ constrains the integral of all past star formation. The local energy output provides the normalization of the first two quoted approaches and consequently cannot be used as an independent check, but the EBL provides an independent test of the three approaches.

The paper is organized as follows. In Section 2 we describe the fossil approach characterized by delayed exponential decay models of cosmological star formation and investigate the resulting color and mean age as a function of characteristic decay time and metallicity. As a result, we construct the 'Fossil' model using two components, bulge and disk, based on the observed colors of galaxies. In Section 3 we consider the star formation history, as predicted by the Fossil model and other *ab initio* theoretical models, and compare it with what is inferred from observation. In Section 4 we discuss the stellar mass density, a time integrated version of the star formation history, which is taken as a consistency test. We then compute the EBL in Section 6 to study whether what is expected from the star formation history is consistent with observations. Conclusions are given in Section 8. When necessary, we adopt a cosmological model with parameters $(\Omega_{\rm M}, \Omega_\Lambda, \Omega_b, h, n, \sigma_8) = (0.3, 0.7, 0.04, 0.7, 1.0, 0.9)$, where $h = H_0/(100 \text{ km s}^{-1} \text{ Mpc}^{-1})$ is the Hubble parameter. Where h is not explicit, $h = 0.7$ is assumed.

2. The Fossil model

Searle, Sargent, & Bagnuolo (1973) showed that the colors of galaxies can be reproduced well by simple exponentially decaying star formation histories, $\dot{\rho}_* = A \exp(-t/\tau)$, where τ is the characteristic decay time. Here we revisit their model with a modern perspective. Throughout this paper, we take $t = 0$ to be the epoch of the Big Bang.

The original model of Searle et al. (1973) has the disadvantage that one has to assume the onset time of star formation by hand, increasing the number of free parameters. Therefore we adopt the delayed exponential model,

$$\dot{\rho}_* = A\,(t/\tau)\exp(-t/\tau). \tag{1}$$

This model has a desirable feature that the SFR vanishes at $t = 0$, and it has a peak at $t = \tau$ followed by an exponential tail with a characteristic time-scale τ. The model with a very small value of τ resembles the instantaneous burst at $t = 0$, and the one with $\tau \sim t_H$ (Hubble time) resembles the model with a constant SFR. The delayed exponential model has the same minimal number of free parameters as the Searle et al. (1973) model, a time-scale τ and a normalization A. Good agreement with other approaches, as we will show later, justifies the use of this functional form for the Fossil model.

Figure 1 shows the delayed exponential models of star formation history as functions of cosmic time (panel [*a*]) and redshift (panel [*b*]) for different values of τ as described in the caption. The normalization A is adjusted so that the integral of the SFR,

$$\int_0^{t_0} \dot{\rho}_* dt / \rho_{\rm crit} = 0.004, \tag{2}$$

where $\rho_{\rm crit}$ is the critical mass density and t_0 is the current age of the universe. The *thick blue solid* line is a composite two population model with $\tau = 1.5\,$Gyr and $4.5\,$Gyr which will be described below.

We note that the integral of SFR (Equation [2]) is not equal to the stellar mass density observed today because of gas recycling, i.e., gas lost by aging stars. The recycling fraction R, defined to be the ratio of the amount of recycled gas to the total amount of gas that was initially converted into stars, depends on the IMF and is a function of time. We show the recycling fraction in Figure 2 computed using the population synthesis model of Bruzual & Charlot (2003, hereafter BClib03). This shows $R \simeq 0.45$ at $t = 13.5\,$Gyr for the Chabrier (2003) IMF integrated from 0.01 to $100\,M_\odot$[1]. In other words, approximately 55% of the initial gas remains in stars and stellar remnants (45% in shining stars and 10% in remnants, i.e., white dwarfs, neutron stars and black holes, for which BClib03 assumes the mass, $0.55, 1.4$, and $2.0\,M_\odot$, respectively.) Therefore the normalization given by Equation (2) corresponds to the stellar mass density $\Omega_\star(z=0) \approx 0.0022$. We note that the recycling fraction of the SSP for the Salpeter IMF ($0.1 - 100\,M_\odot$) is $R = 0.32$ at $t = 13.5\,$Gyr.

We then compute the colors of galaxies for each model using BClib03 with the Chabrier IMF. The delayed exponential models give $u-g$ and $g-r$ colors as shown in Figure 3a at $t_0 = 13.5\,$Gyr. The three lines stand for metallicities: $Z/Z_\odot = 0.2$ (*black open squares*), 1.0 (*blue solid triangles*), and 2.5 (*red open triangles*), with τ varying along the line from top (0.1 Gyr) to bottom (10 Gyr) as indicated in the legend. Also shown as contours is the color distribution of SDSS galaxies taken from Figure 7 of Blanton et al. (2003b).

The histogram (normalized arbitrarily) of the SDSS galaxy color projected onto each axis is shown in Figure 3b, with double Gaussian fits by eye. The two rectangular boxes delineated with dots indicate the locations of the Gaussian peaks with the width twice the dispersion: $u-g = 0.94 \pm 0.25$ and $g-r = 0.43 \pm 0.14$ for the blue peak, and $u-g = 1.6 \pm 0.25$ and $g-r = 0.88 \pm 0.07$ for the red peak. Much has been said of the bimodal color distribution seen in the local galaxies from the SDSS (Strateva et al. 2001; Blanton et al. 2003b; Kauffmann

[1]BClib03 integrates the Chabrier IMF from 0.1 to $100 M_\odot$. We applied the correction for brown dwarfs that reduces R from BClib03 by a factor of 0.94.

et al. 2003; Baldry et al. 2004; Balogh et al. 2004; Brinchmann et al. 2004). The two distinct distributions correspond to non-star forming and star-forming galaxies, but roughly also to the redder spheroid-dominated component and the bluer disk galaxies. This is the concept first noticed by Baade (1944) in his proposal of the two population model. He also pointed out that the two types of stellar populations had been recognized as early as 1926 by Oort (1926).

We represent the peaks of SDSS galaxy color distribution with two parameters $(\tau, Z/Z_\odot)$. Figure 3a shows that the models with $\tau = 1.5\,\mathrm{Gyr}$ and $4.5\,\mathrm{Gyr}$ fit the colors of the spheroid and disk components reasonably well, respectively, and the variation of metallicity gives a further tuning. We find that it is difficult to realize the colors $(u-g, g-r) = (1.6, 0.9)$ with BClib03 even when we push the metallicity to $Z/Z_\odot = 2.5$, which is unlikely to be a representative of spheroid component even if the most massive elliptical galaxies may have such a high metallicity. We present the stellar mass weighted mean metallicity for spheroids (early type galaxies and bulges of disk galaxies) of different morphological types in Table 4, as calculated in Appendix A. As a result, we construct a composite 'Fossil' model — we call it Fossil because it is based on the fossil evidence in the present universe, i.e., colors of galaxies — with the parameters $(\tau\,[\,\mathrm{Gyr}], Z/Z_\odot) = (1.5, 1.5)$ for the spheroid component and $(4.5, 0.8)$ for the disk component [2]. These parameters are indicated by the *asterisks* in Figure 3b. The blue asterisk for the disk component is located at the center of the box, but the red asterisk for the spheroid is slightly off to the corner. The mass-weighted mean metallicity of the spheroid component we obtain in Table 4 is $1.3\,Z_\odot$, but in order to keep the red asterisk within the dotted box in Figure 3b, we choose to adopt $1.5\,Z_\odot$ for the spheroid component.

Next, we determine the normalization of the two components. We choose to normalize each component by requiring a match of the energy output in K- and r-bands with observations (see Appendix B). Our normalization corresponds to the bulge(spheroid)-to-disk stellar mass ratio $(M_b/M_d) = 1.35$, or equivalently $M_b : M_d = 57\% : 43\%$. An alternative method to determine the normalization uses the bulge-to-disk luminosity ratio and the mass-to-light ratio for each morphological type of galaxies, as outlined in the caption of Table 1; this gives $(M_b/M_d) = 1.9$, or $M_b : M_d = 66\% : 34\%$. Given the uncertainties involved, we consider the bulge stellar mass fraction of $55-70\%$ to be observationally allowed. For this work we adopt 57% obtained in Appendix B, but the exact value is not important to the major conclusions.

[2]Here we are representing the entire galaxy population with two delta functions on the color-color plane. It is possible in the future to extend Figure 3 into a three dimensional color space by adding another color as a z-axis, and assign a set of parameters (τ, Z) to every grid cell in the 3-d color space. That would be a more smooth, continuous representation of stellar mass distribution in the color space.

Figure 4 shows the mass-weighted mean stellar age for the delayed exponential model, calculated as

$$t_{\rm age} = t_0 - \left(\int_0^{t_0} t\, \dot{\rho}_\star(t)\, dt \;/\; \int_0^{t_0} \dot{\rho}_\star(t)\, dt \right). \tag{3}$$

The mean age of disk stars ($\tau = 4.5\,$Gyrs) turns out to be $t_{\rm age} = 7\,$Gyrs, which is consistent with the observational estimate of $5 - 7$ Gyrs (Rocha-Pinto et al. 2000; Robin et al. 2003; Naab & Ostriker 2006). We note that our estimate includes the stellar remnants. Had one omitted the contribution from stars that died in the history of the universe, then the mean age would be younger by approximately 0.8 Gyr, as indicated by the arrows. The main properties of our Fossil model at the present epoch are summarized in Tables 2 and 3. It may be helpful to note that the historical development of the present distribution of galaxies is of no import for the Fossil model. It makes no difference at all to the accounting if we had dry, wet, or no mergers. All that matters is that the local SDSS inventory of a representative volume enables us to estimate the age distribution of star formation.

3. Cosmic star formation history

In Figure 5, we show the cosmic SFR density as a function of redshift. The *blue solid* line is the Fossil model described in the previous section, and the *black short-dash long-dash* line shows the result of a new Eulerian TVD hydrodynamic simulation. This simulation has a comoving box size of $85h^{-1}$ Mpc and 1024^3 hydrodynamic mesh, and the code is similar to the one used by Cen, Nagamine, & Ostriker (2005) and Nagamine et al. (2004). The physical cell size is $83/(1+z)\,h^{-1}$ kpc. The mean baryonic mass per cell for this simulation is $m_{\rm gas} = 3.63\times 10^6\,h^{-1}M_\odot$ and the dark matter particle mass is $m_{\rm DM} = 1.58\times 10^8\,h^{-1}M_\odot$ (512^3 particles). The cosmological parameters are $(\Omega_{\rm M}, \Omega_\Lambda, \Omega_b, h, n, \sigma_8) = (0.31, 0.69, 0.048, 0.69, 0.97, 0.89)$. The TVD result is extracted from the simulation without additional processing except for the boxcar smoothing over ± 3 bins in the redshift axis. The amount of gas converted into stars is a direct output of the simulation, so there is no uncertainty as to stellar IMF and no freedom for the normalization. For the details on the star formation and supernova (SN) feedback prescription, we refer the readers to Cen & Ostriker (1993); Nagamine et al. (2001b); Cen et al. (2005).

We also consider two other models: one from Hernquist & Springel (2003, H&S model) who derived an analytic approximation for the SFR history as a function of redshift based on their cosmological Smoothed Particle Hydrodynamics (SPH) simulations. The H&S model shown in *green long-dashed* line takes the form

$$\dot{\rho}_\star = \dot{\rho}_\star(0) \frac{\chi^2}{1 + \alpha(\chi - 1)^3 \exp\left(\beta\chi^{7/4}\right)}, \tag{4}$$

where $\chi(z) \equiv (H(z)/H_0)^{2/3}$. With star formation and feedback models adopted in Springel & Hernquist (2003a), the parameters are $\alpha = 0.012$, $\beta = 0.041$, and $\dot{\rho}_\star(0) = 0.013\,\mathrm{M}_\odot\ \mathrm{yr}^{-1}\ \mathrm{Mpc}^{-3}$. The normalization is fixed to give the local SFR density (Hernquist & Springel 2003).

The other model represented by *red short-dashed* line is the semi-analytic model GALFORM by Cole et al. (2000, hereafter SA model). The cosmological parameters that H&S and SA adopted $(\Omega_\mathrm{M}, \Omega_\Lambda, \Omega_b, h, n, \sigma_8) = (0.3, 0.7, 0.04, 0.7, 1.0, 0.9)$, differ slightly from those of the TVD simulation. We confirmed that this slight difference is not important for our analyses. Table 3 summarizes the basic characteristics of these models.

For the observational data shown in Figure 5, we assume the Chabrier IMF $(0.01 - 100 M_\odot)$. The UV luminosity densities ρ_UV are converted into SFR by

$$\rho_\mathrm{UV}\ [\mathrm{erg\ s^{-1}\,Hz^{-1}\,Mpc^{-3}}] = C\,\dot{\rho}_\star\ [M_\odot\,\mathrm{yr}^{-1}\ \mathrm{Mpc}^{-3}], \tag{5}$$

where the parameter C can be derived from BClib03 as

$$C = 1.24 \times 10^{28} \tag{6}$$

for an exponentially decaying star formation history with $\tau = 5\,\mathrm{Gyr}$ for the Chabrier IMF and solar metallicity. Here ρ_UV is computed by averaging the flux over $\pm 150\,\text{Å}$ centered at $\lambda = 1500\,\text{Å}$ at age $t = 10\,\mathrm{Gyr}$. The parameter C depends on the age of the stellar population and reaches a plateau after $t \sim 100\,\mathrm{Myr}$ for $\tau \gtrsim 1\,\mathrm{Gyr}$ models. The value in equation (6) differs by a factor 1.6 from the value given by Madau, Pozzetti, & Dickinson (1998) who performed the same calculation for the Salpeter IMF $(0.1 - 100\,M_\odot)$.

The correction due to dust obscuration is important. For observations of nearby universe, the Balmer emission lines (Gallego et al. 1995; Tresse & Maddox 1998; Hopkins et al. 2000; Pascual et al. 2001; Tresse et al. 2002; Nakamura et al. 2004) can be used to estimate the SFR with reasonable reliability at $z \sim 0$. For higher redshift, where SFR is derived from the UV light, estimates of extinction are more uncertain. Steidel et al. (1999) took $E(B-V) = 0.15$, somewhat smaller than the value inferred for the local galaxies. At some point at high redshift, the dust content should start decreasing as a function of increasing redshift, but whether this is seen towards higher redshift or not is controversial even today. Bouwens et al. (2005) suggest a modest decline in the dust extinction effect from $z = 3$ to $z = 6$, but Thompson et al. (2006) indicate the extinction correction of a factor of 5 at $z = 6$, which differs little from that at $z = 3 - 4$. In this situation we must be content with with our fiducial choice of the conventional prescription of Steidel et al. (1999) that the SFR are corrected by factors of 2.7 ($z < 2$) and 4.7 ($z > 2$), as also supported by the subsequent work by Reddy & Steidel (2004). We apply this correction to most of the data (after removing the corrections by individual authors), keeping in mind that varying dust extinction

as a smooth function of redshift is needed to obtain more reliable estimates of SFR. Note that the faint-end slope of the luminosity function at high-redshift is poorly constrained and SFRs are derived under different assumptions (we do not dare to standardize them except for extinction corrections), which we review briefly in what follows.

Steidel et al. (1999, filled pentagons at $z = 3, 4$) derived their UV luminosity density by integrating the luminosity function with the faint-end slope of $\alpha = -1.6$ down to $0.1L^*$. We take the SFR from their Fig.9, and convert it to the Λ cosmology. Giavalisco et al. (2004, open triangles at $z = 3-6$) integrated the Schechter fit with $\alpha = -1.6$ to $0.2L^*$. Ouchi et al. (2004a, filled circles) integrated the luminosity function with $\alpha = -2.2$ to $0.1L^*$. Bouwens et al. (2005, filled square at $z = 6$) integrated their Schechter fit with $\alpha = -1.74$ to $0.04L^*_{z=3}$. Their sample goes to the faintest magnitude compared to others, yet the result still indicates some decline in SFR density from $z = 3$ to $z = 6$ by a factor of ~ 0.7. Thompson et al. (2006) performed the SED fitting to the 6 photometric broadband measurements by ACS and NICMOS of the Hubble Ultra Deep Field determining the extinction for each sources. They then utilized the star formation intensity distribution function (Lanzetta et al. 2002) to correct for the surface brightness dimming effect. Their result is consistent with the earlier result by Thompson (2003). Here we take the extinction uncorrected data listed in their Table 2 and applied our correction as mentioned above. Since their errors are large and the error bars overshoot to the outside of the plotted range of Figure 5 when put on our version of data points, here we omitted the error bars for this data.

Extinction corrections are not applied to the data derived from X-ray (Norman et al. 2004) and submillimeter observations Barger et al. (2000, taken from Table 2 of Hopkins (2004)), as they are less subject to dust extinction effects. The data by Heavens et al. (2004) at very low-redshift from the MOPED (Heavens et al. 2000) algorithm already include the correction for dust for each galaxy. The data of Nakamura et al. (2004) are derived from hydrogen Balmer lines including a consistent correction for extinction in individual galaxies. We note that uncertainties for $z \geq 1$ could be much larger than those represented here, while those for lower redshift are probably not too large since dust extinction is constrained well with the use of Balmer lines.

With large uncertainties we discussed in mind, Figure 5 shows a good agreement among the three independent approaches: observed SFR, Fossil model, and *ab initio* models. All estimates agree with each other to within about a factor of two, which is also the size of the scatter in the data. We see some declining trend of the SFR in the SA model at $z > 4$, which contrasts to the other numerical *ab initio* models and the Fossil model that show a roughly constant rate of star formation. Our argument given here should be understood in the sense that if observations would receive too large systematic errors, the consistency with the two

other approaches is endangered.

We also underline the conclusion from the Fossil model that the spheroidal component formed primarily at high-redshift ($z \gtrsim 1.5$), and the majority of the disk stars formed at low-redshift ($z \lesssim 1$). The sum of these two components falls in-between the curves of other models.

A note on the uncertainty due to our poor understanding of star formation is appropriate. The theoretical calculations are most secure in their predictions of the SFR, while the prediction of the electromagnetic output (and the stellar mass density to some extent) do depend on assumptions concerning the stellar IMF. The observational measurements are done for the electromagnetic output and SFR is derived by assuming an IMF, therefore the observational estimates of SFR suffers from the uncertainty in the assumed IMF. Further uncertainty is expected from dust extinction. This is particularly important when we deal with far UV light.

We also remark that the star formation rate in the simulations could depend on the details of the SN feedback prescriptions. If the feedback is turned off in the simulations, the heating of the gas is underestimated and therefore the global SFR density at low redshift is overestimated (i.e., *physical* overcooling of the gas). In the TVD simulation used in this paper and the SPH simulations on which the H&S model is based, the strength of the feedback was set based on the energetic argument of SN explosion and was also calibrated against various observations such as the star formation rate of Lyman break galaxies, metallicities of the Lyα forest and intra-cluster gas, and the galactic wind speeds observed in starburst galaxies. The current spatial resolution of the TVD simulation (physical cell size of $83/(1+z)\,h^{-1}\,\mathrm{kpc}$) is not adequate to resolve the details of the inner structure of galaxies, but the overall star formation rate can be simulated with some confidence as the energetics are faithfully simulated on scales slightly larger than the real galaxies.

4. Stellar mass density

As we noted, the integral of SFR from $t = 0$ to t_0 is not equal to the stellar mass density, as the gas recycles into the interstellar medium. Figure 6a shows the evolution of the global stellar mass density $\Omega_\star$ as a function of redshift. The model results take account of the time-varying recycling fraction derived from BClib03. All results assume the Chabrier IMF ($0.01 - 100\,M_\odot$).

The values of $\Omega_\star$ at $z = 0$ after the gas recycling correction are 0.0021, 0.0028, 0.0021, and 0.0023 for the Fossil, TVD, H&S, and SA models, respectively (see Table 3). The

empirical estimates converges to $\Omega_\star \approx (2.4 - 3.6) \times 10^{-3}$ with the Chabrier IMF ($0.01 - 100\,M_\odot$), or $(1.8-3.9)\times10^{-3}$ taking the errors into account. The model values are consistent with this range with a lower value favored. We remark that the conversion factor for $\Omega_\star$ from Salpeter IMF (mass range $0.1 - 100\,M_\odot$) to Chabrier IMF ($0.01 - 100\,M_\odot$) is 1.4 for the same amount of luminosity output at $M > 1M_\odot$. The data are taken from Cole et al. (2001, *green filled circle)*, Panter et al. (2004, *black open circle*, the size of the claimed error bar is comparable to the symbol size), Fukugita & Peebles (2004, *black inverted triangle)*, Kochanek et al. (2001, *black open pentagon*, slightly offset from $z = 0$ for clarity), and Bell et al. (2003, *solid pentagon).*

The situation is different for the stellar mass for higher z. The figure compares the model curves with the observational analyses given by Rudnick et al. (2003, *magenta filled squares*, Table 2), Dickinson et al. (2003, *cyan open stars)* Brinchmann & Ellis (2000, *red open squares)*, Fontana et al. (2004, *blue open crosses*, Table 4, 'observed' column), and Glazebrook et al. (2004, *black filled triangles)* all transformed to the Chabrier IMF.

At $z \gtrsim 1$ the observational estimates all fall significantly short of the model. Roughly speaking, all models predict that $\sim 60\%$ of the present stellar mass was formed by $z = 1$, whereas the observation indicates it is as small as $20 - 30\%$, a gross disagreement, as also discussed by Nagamine et al. (2004) earlier. We emphasize that this is likely to be an observational problem, since the straightforward integration of the empirical star formation rate, corrected for the recycling factor, yields a stellar mass substantially larger than what is observed, indicating a gross underestimate of the stellar mass in high-redshift galaxies in currently available analyses. We note that possible errors in extinction corrections for $z \geq 1$ galaxies do not solve this problem.

5. Metal mass density

Given the star formation histories, one can compute the metal mass density as a function of redshift as

$$\dot{\rho_\star} = Y \dot{\rho_Z}, \tag{7}$$

where we take $Y = 0.023$ using the prescription of Arnett (1996, Section 14.4) adjusted to the Chabrier IMF. (This value corresponds to the Searle-Sargent yield $Y/(1 - R) = 0.042$.) The evolution of metal mass density is shown in Figure 7 together with empirical estimates.

At $z = 0$, all models agree well with the estimate by Fukugita & Peebles (2004), $\Omega_Z = (0.8 \pm 0.25) \times 10^{-4}$ (eq.[94]), which excludes the contributions from stellar remnants but includes those from warm galactic halos. Dunne et al. (2003, Table 1) give an estimate

higher than Fukugita & Peebles (2004) by 50%, and the TVD model is consistent with their central value. Other model predictions are consistent with Dunne et al.'s estimate at its lower edge.

Dunne et al. (2003) also give an estimate of the metal abundance at $z = 2.5$ including damped Lyα systems. The models are consistent with their estimate at $z = 2.5$, although the TVD and H&S model lie somewhat above the given error bar. Bouché et al. (2006) and Prochaska et al. (2006) presented metal abundance from high-z galaxies and damped Lyα systems lower than Dunne et al. They are, however, taken as lower limit, first because of missing contributions of faint galaxies as discussed by the authors, but perhaps more importantly by the omission of metals in warm galactic halos, which may contribute by additional 50-100%. Therefore we consider that the "missing metal problem" is not really a problem.

6. Energy in the radiation

The last test concerns the consistency with the energy in the radiation field, the product of stellar evolution. To estimate EBL we use the compilation of Hauser & Dwek (2001) for the source of observations. We write the integral of the flux over the range between λ_1, and λ_2 (in μm), as

$$I_{\rm EBL}[\lambda_1, \lambda_2] \equiv \int_{\lambda_1}^{\lambda_2} \nu I_\nu \, d\ln\nu \tag{8}$$

in units of nW m^{-2} sr^{-1}. For the optical to the near IR region direct observations of extragalactic background yield $I_{\rm EBL}[0.16, 3.5] \approx 60$, whereas the integration of galaxy counts give $I_{\rm EBL}[0.16, 3.5] \approx 18$. We may take these two numbers as upper and lower limits, since the former is derived from difficult observations that are apt to be contaminated with local emission, while the latter would miss light from the outskirts of galaxies. For the far IR that is dominated by dust we adopt Hauser-Dwek's estimate: $I_{\rm EBL}[3.5, 140] = 11 - 58$, where the upper value comes from fluctuation measurements and the lower from integration of resolved sources. Measurements are more secure for the submillimeter region: $I_{\rm EBL}[140, 1000] = 15 \pm 2$. Adding the three together, we take the total obscured EBL flux to be

$$I_{\rm EBL}[0.16, 1000] = 42 - 135 \ {\rm nW\,m^{-2}\,sr^{-1}}, \tag{9}$$

which ranges over a factor of 3. We avoid quoting the central value, since this range represents predominantly systematic uncertainties and what value should be taken as central is rather a matter of interpretation.

The bolometric EBL and the comoving bolometric luminosity density at redshift z, $j_{\rm bol}(z)$, are related by

$$I_{\rm EBL} = \left(\frac{c}{4\pi}\right)\int_0^\infty j_{\rm bol}(z)\left|\frac{dt}{dz}\right|\frac{dz}{1+z} \quad (10)$$

$$= 9.63\times10^{-8}h^{-1}\int_0^\infty\left[\frac{j_{\rm bol}(z)}{L_\odot{\rm Mpc}^{-3}}\right]H_0\left|\frac{dt}{dz}\right|\frac{dz}{1+z} \quad [\,{\rm nW\,m^{-2}\,sr^{-1}}\,], \quad (11)$$

where

$$H_0\left|\frac{dt}{dz}\right| = \frac{1}{(1+z)\sqrt{\Omega_{\rm M}(1+z)^3+\Omega_\Lambda}} \quad (12)$$

for a flat Λ universe, and $j_{\rm bol}(z)$ can be obtained by

$$j_{\rm bol}(t) = \int_0^t \dot\rho_*(\tau)\,[L_{\rm bol}(t-\tau)/M]\,d\tau, \quad (13)$$

with $\dot\rho_*(\tau)$ the comoving SFR density in units of $M_\odot\,{\rm yr}^{-1}\ {\rm Mpc}^{-3}$, and $L_{\rm bol}(t)/M$ $({\rm erg}\,M_\odot^{-1})$ the bolometric luminosity per mass of a stellar population with age t.

6.1. Bolometric luminosity density

Figure 8a shows the comoving bolometric luminosity density as a function of redshift for the Fossil, TVD, H&S, and SA models. For the latter three models a solar metallicity is assumed. Figure 8b shows the spheroid and disk components separately for the Fossil model. We use the bolometric electromagnetic output to minimize uncertainties due to corrections for dust obscuration.

We take Kashlinsky (2005)'s summary for observed luminosity density at the present epoch: $j_{\rm bol}(0.2{-}2\mu{\rm m}) = (9.8{\pm}1.2){\times}10^{41}\,h\,{\rm erg\,s^{-1}\,Mpc^{-3}}$ and $j_{\rm bol}(12{-}100\mu{\rm m}) = (1.5{\pm}0.3){\times}10^{41}\,h\,{\rm erg\,s^{-1}\,Mpc^{-3}}$. Adding these two and using $h = 0.7$, we obtain $j_{\rm bol}(0.2-100\mu{\rm m}) = (3.98{\pm}0.43){\times}10^8 L_{\odot,{\rm bol}}\,{\rm Mpc^{-3}}$. Note that the energy density in the range of the gap, $2{-}12\mu$m is expected to be small from the observations of the EBL. We expect the contribution from $\lambda > 100$ μm as $I_{\rm EBL}[120,1000] = 10-15$ nW m^{-2} sr^{-1} (Hauser & Dwek 2001; Kashlinsky 2005). This yields $j_{\rm bol}(0.2-1000\mu m) = (4.4\pm0.5)\times10^8 L_{\odot,{\rm bol}}\,{\rm Mpc^{-3}}$. Being conservative on the error, we adopt

$$\log j_{\rm bol} = 8.6\pm0.1, \quad (14)$$

as our estimate of the bolometric luminosity density at $z = 0$, which is shown in Figure 8. This estimate agrees with that of Bell et al. (2003, see their Fig.15). It is interesting that there is no discrepancy amongst the models and between the models and observations at $z = 0$, while the model predictions are rather divergent to one order of magnitude at high redshift.

6.2. EBL

From the bolometric luminosity density shown in Figure 8, we compute the total EBL using equation (11) as a function of redshift for each model of cosmic star formation history. Our calculation does not include the contribution from AGN, which amounts to 7%, as estimated in Nagamine et al. (2006, in preparation). The model predictions are all convergent on $I_{\rm EBL} \approx 37 - 51$ nW m^{-2} sr^{-1} at $z = 0$, which are to be compared with the observation, $I_{\rm EBL}[0.16, 1000] = 42 - 135$ nW m^{-2} sr^{-1} quoted above. This indicates that the models are consistent with the observation only at its lower edge, suggesting that the current EBL observations might still be contaminated from non-cosmological sources, whereas the integration over resolved sources yields the value theoretically expected [3]. The model prediction would even undershoot the observations if the Salpeter IMF were adopted.

We may have another look at this problem by considering the ratio of the EBL to the bolometric luminosity density at $z = 0$. We define the dimensionless parameter

$$\eta_\star \equiv \left(\frac{4\pi}{ct_H}\right)\frac{I_{EBL}}{j_{\rm bol}} = 7.293 \times 10^6 \ \frac{I_{EBL}\,[{\rm nW\,m^{-2}\,sr^{-1}}]}{j_{\rm bol}\,[L_{\odot,{\rm bol}}\ {\rm Mpc^{-3}}]}, \tag{15}$$

where $t_H \equiv 1/H_0$ is the Hubble time. This parameter compares the EBL with the luminosity density multiplied by the Hubble time, and the advantage is that it is independent of uncertainties in the stellar IMF provided that it does not vary as a function of time. From Figures 8 and 9, we compute $\eta_\star$, as shown in Figure 10. The results are indicated by arrows, and the solid line shows $\eta_\star$ as a function of τ for the delayed exponential models. They are compared with the observation indicated by shades that ranges from $\eta_\star = 0.61$ to 3.11 from equations (9) and (14). All models result in $\eta_\star = 1.0 \pm 0.2$, which is consistent with only the lower part of the apparently observed range. Therefore, the problem is IMF independent.

7. Inconsistency among observations

The evidence we have discussed in the previous sections indicate that we now have reasonable understanding of the cosmic star formation history. There are, however, two items that do not fit well to the scenario. They are the stellar mass density at $z \gtrsim 1$ and the EBL from direct measurements of sky.

We showed that the observationally derived stellar mass densities at $z \geq 1$ are significantly smaller than the prediction of all the models, while the models agree well with the

[3]See Note Added in the end of this paper.

observed SFR up to $z \sim 5$. This means that the observational data of SFR and stellar mass density are inconsistent with each other. The integration of SFR, model or observation, gives the correct stellar mass density at $z = 0$, which is a strong constraint. Hence, this is clearly an observational problem that observations underestimated the stars locked in galaxies at $z \gtrsim 1$. Is it possible that the estimates of the stellar mass density are correct at all redshift and the SFR is mis-estimated? This is unlikely, because, to give the curve of the observed stellar mass density at $z \gtrsim 1$, SFR must decline sharply from $z \approx 0.5$ to higher redshift while the SFR density $z < 0.5$ is substantially higher than is measured. Therefore, we may ascribe the problem to underestimates of the stellar mass density at $z \gtrsim 1$, presumably from poor understanding of the optical/NIR luminosity functions for sub-luminous galaxies..

The observation of EBL harbors another problem. All model results are consistent with the EBL only when we take the value obtained by integration of resolved sources, in *both* optical and infrared bands. In the optical band, direct measurements (Bernstein et al. 2002) give the EBL 3 times that from integration of resolved sources (Madau & Pozzetti 2000; Totani et al. 2001). This factor becomes 5 in the infrared (see Hauser & Dwek 2001, and references therein). The directly measured EBL in either of the cases gives too bright a flux to be accounted for. This conclusion does not depend on cosmological theories, nor on the IMF. It is a result of requiring consistencies between stellar mass density today and the light that has been emitted by those stars with subsidiary information concerning the star formation history inferred from the Madau diagram. Therefore this is also an observational problem possibly due to insufficient subtraction of the Zodiacal light (see also Kneiske et al. 2002; Mattila 2003) [4]. Finally there is an inconsistency between the observed value of the luminosity density and the observed EBL for any plausible star formation history.

One may argue for the possibility that EBL in the infrared is actually bright as a result of emission from high-redshift stars which are not included in our modeling. We consider that this is unlikely, since we do not find at $z = 0$ extra stars that were responsible for such emission at high-redshift, and the amount of stars at $z = 0$ is well documented. If there were very massive stars such as Population III (e.g. Cambresy et al. 2001; Matsumoto 2001; Cooray et al. 2004; Kashlinsky et al. 2004; Kashlinsky 2005; Matsumoto et al. 2005), these objects would die quickly and will not be counted as stars at the present epoch. However there are several difficulties with this hypothesis, such as much higher SFR at $z > 7$ than at $z = 3 - 5$ (Fernandez & Komatsu 2005), possibility of over-enriching the intergalactic medium by metals (Salvaterra & Ferrara 2003; Ricotti & Ostriker 2004), physically unrealistic absorption-corrected spectra of distant TeV blazars (Dwek et al. 2005b,a), and

[4]See Note Added in the end of this paper.

overproduction of soft X-ray background (Madau & Silk 2005).

8. Conclusions

We have considered three physically motivated approaches: one with *ab initio* theoretical models that are constrained basically by the observation of WMAP at $z \approx 1000$, another with the Fossil model that uses theory of stellar evolution constrained by the SDSS observation at $z \approx 0.1$, and yet another purely from observations at $z = 0 - 6$. We considered various physical quantities that witness the star formation history: stellar mass density, luminosity density, bolometric luminosity density and EBL, and we found a general agreement among results from these three approaches within the errors the current observations indicate. In particular, we found that the exceedingly simple Fossil model having two populations with parameters adjusted to the SDSS observation — an update of the Searle et al. (1973) model — provides a very effective description of the star formation history predicted by *ab initio* theoretical models, and it also exhibits a good fit to the suite of tests we have applied.

The only exception was in the stellar mass density at high redshift, where not only the Fossil model but all models predict higher values than the observationally derived ones. The observational results do not look consistent with what are inferred from the empirical Madau plot. This is not a matter of normalization of the star formation histories shown in Fig. 5, since the data on stellar mass density at $z = 0$ are now well converged, and they are consistent with the integral of the SFR when the gas recycling is taken into account (see also Fukugita & Peebles 2004). If the dust extinction effect were significantly weaker than what we adopted here and the normalization of the SFR history were brought down in such a way that the integral of the SFR is consistent with the current data on stellar mass density at $z > 1$, such a SFR history would be inconsistent with the measured stellar mass density at $z = 0$. Therefore, we regard the disagreement in the stellar mass density at $z > 1$ between the models and observations as an observational problem.

We also noted that the predictions of the EBL from the models all converged at the lower edge of the best current observations, giving $I_{\rm EBL} = 43 \pm 7\,{\rm nW\,m^{-2}\,sr^{-1}}$. This implies that the true EBL flux is presumably close to the value obtained by integrating over resolved sources.

Before proceeding further, we should ask if an incorrect modeling of the stellar IMF could be the culprit. The number and mass in stars less massive than $0.4M_\odot$ are quite uncertain as they do not significantly affect observed spectral properties and their contribution to dynamically determined mass estimates is obscured by the uncertainties in the dark mat-

ter component. For our analysis we consistently adopted the Chabrier IMF ($0.01 - 100 M_{\odot}$). Let us now suppose that, due to a higher than expected fraction of low-mass stars (as compared to the Chabrier IMF), the effective mass-to-light ratio values were all to be increased by a factor of μ ($\mu \approx 1.6$ for the Salpeter IMF; values of $\mu < 1$ are also permitted if there were a even stronger turn-over of the stellar number density with decreasing mass as compared to the Chabrier IMF). This change would alter the theoretical models by reducing the EBL by a factor of about μ. The observed values of EBL would of course be unchanged. Thus, increasing the contribution of low-mass stars as compared to the Chabrier IMF would exacerbate the problem of under-predicting the EBL for all the models. On the other hand, reducing the contribution of low-mass stars even more so than the Chabrier IMF would ease the disparity between the predicted and observed EBL. But then the models would overpredict the present-day luminosity density in various bands and disrupt the rough agreement with the observed values that we found in Table 3. Therefore no simple adjustment of the stellar IMF can be made to remove all discrepancies. In addition, the parameter $\eta_{\star}$ was constructed (Equation [15]) in a fashion so as to avoid uncertainties in the stellar IMF and it too shows a discrepancy between observed and predicted value. Therefore it seems inevitable that the models of cosmic star formation history that we considered in this paper cannot account for a total optical-to-IR EBL of ~ 100 nW m^{-2} sr^{-1}. We would suggest that the direct observation of the EBL in sky may still be contaminated by local emissions. If future observations would converge to a higher EBL value, as the current direct EBL observations indicate, we would get into a trouble in modeling the history of galaxies: we may have to invoke additional components, such as mini black holes or population III stars with a top-heavy IMF that are not included in the current modeling as discussed in Section 7.

An interesting feature of our Fossil model is that it predicts that the spheroid component formed predominantly at $z \gtrsim 1.5$, and the disk component formed mostly at $z \lesssim 1$. The early formation of the spheroidal component is consistent with some recent direct numerical simulations (e.g., Abadi et al. 2003; Naab et al. 2005). This agrees with the observational knowledge known for some time (e.g., Fukugita et al. 1996) and the early work by Searle et al. (1973) and predecessors. Although the current *ab initio* models cannot distinguish between these two components, the Fossil model provides one example how the total population can be separated into the two population, consistently with observations. As a consequence of the early formation of the spheroidal component, our models clearly indicate a relatively constant star formation rate from $z = 7$ to $z = 2$. It will be interesting to see if this prediction is confirmed or refuted by ongoing observational programs.

We also note that the rapid decline of the spheroid formation from $z = 3$ to $z = 1$ in the Fossil model works in favor of having a population of Extremely Red Objects (EROs; e.g. McCarthy 2004) at $z = 1$ as found by recent observations (e.g. Cimatti et al. 2004;

Glazebrook et al. 2004; McCarthy et al. 2004). The existence of these EROs were first regarded as a challenge to the hierarchical CDM models (Somerville et al. 2004), but was later shown (Nagamine et al. 2005b,a) that the overall space density of EROs could be accounted for in cosmological hydro-simulations. Having a high value of SFR density at high-redshift ($z \geq 4$) as our models (except the SA model) helps to resolve the issues with the existence of high-redshift EROs.

We conclude that the agreement among the three different approaches, as summarized in Table 3, is encouraging, and that the Fossil model provides a simple effective description of cosmological star formation history with very few free parameters. Furthermore, the general agreement between the TVD, H&S, and the Fossil model suggests that the cosmological hydrodynamic simulation based on a cold dark matter model is providing a reasonably accurate picture of cosmological star formation history without a fine tuning of input parameters.

We thank Thorsten Naab, Alice Shapley, and Michael Strauss for useful comments on the manuscript. We are grateful to Alan Heavens and Armin Gabasch for providing us with the SFR data points in electronic form. This work was supported in part by grants NAG5-13381, AST 05-07521 and NNG05GK10G. MF received support by Grant in Aid of the Ministry of Education at the University of Tokyo and by the Monell Foundation at the Institute for Advanced Study. The cosmological TVD hydrodynamic simulation was carried out at the National Center for Supercomputing Applications (NCSA).

NOTE ADDED:

After the submission of our paper, Aharonian et al. (2006) published an important upper limit to the NIR background from the HESS observation of high energy gamma rays from two blazers, H2356−309 and 1ES1101−232. The absence of absorption of gamma rays excludes the high value of EBL inferred from NIR fluctuation measurements, while the EBL from the source count is consistent with the observation. This agrees with our conclusion derived from the analysis given in Sect. 5.2. We also note that the source count recently measured with Spitzer (Dole et al. 2006) agrees with the EBL we concluded.

A. Mean metallicity of bulge

We calculate the mass-weighted mean metallicity of the early type galaxies and the bulge component of spiral galaxies by

$$\langle Z \rangle = \frac{\int Z(M)\, M\, \frac{dN}{dM}\, dM}{\int M\, \frac{dN}{\mathrm{d}M}\, dM} \tag{A1}$$

$$= \frac{\int Z(L)\, L\, \left(\frac{M}{L}\right) \frac{dN}{dL}\, dL}{\int L\, \left(\frac{M}{L}\right) \frac{dN}{dL}\, dL} \tag{A2}$$

$$= \frac{\int Z(L)\, L^{1.14}\, \frac{dN}{d\log L}\, d\log L}{\int L^{1.14}\, \frac{dN}{d\log L}\, d\log L}, \tag{A3}$$

where $Z(M)$ and $Z(L)$ are the metallicity of the bulge component as a function of stellar mass M and luminosity L. In equation (A3) we used the scaling $(M/L) \propto L^{0.14}$ for the stellar mass-to-light ratio of late-type galaxies (Bernardi et al. 2003; Vale & Ostriker 2004). We estimate the function $Z(L)$ from the relation between metallicity and velocity dispersion,

$$[Z/\mathrm{H}] = 0.53\,(\log\sigma - 2.173) + 0.15 \tag{A4}$$

obtained by Nelan et al. (2005). Using the Faber-Jackson relation (Faber & Jackson 1976),

$$\sigma = \frac{220}{\sqrt{2}} \left(\frac{L}{L^*}\right)^{0.25} \ \mathrm{km\ s^{-1}}, \tag{A5}$$

we obtain

$$Z(L) = 0.13\, \log\left(\frac{L}{L^*}\right) + 0.16. \tag{A6}$$

We assume the same relation for bulges of late type galaxies.

We take r-band luminosity functions (LFs) of different morphological types of galaxies from Nakamura et al. (2003), and scale down the luminosity of S0/a-Sb, Sbc-Sd galaxies by factors of of 0.40 and 0.24 (see Table 1), respectively, to exclude the contribution from the disk component. The result of the integral (A3) is presented in Table 4.

A caveat is that Equation (A6) may not be entirely appropriate for the bulges of late types galaxies, because the relation suggests the metallicity of the bulge of the Milky Way would be super-solar (0.5 dex), while observations suggest sub-solar metallicity (-0.5 dex) for bulge stars of the Milky Way (e.g., Freeman & Bland-Hawthorn 2002). We may have overestimated the mean metallicity for bulges of disk galaxies.

B. Determination of the Normalization of the Fossil Model

The disk and the bulge components of the Fossil model are normalized to the observed luminosity densities $j_{K,tot} = 4.1 \times 10^8\, h_{70} L_{\odot,K}\,\mathrm{Mpc}^{-3}$ (Bell et al. 2003; Cole et al. 2001) and $j_{B,tot} = 1.3 \times 10^8\, h_{70} L_{\odot,B}\,\mathrm{Mpc}^{-3}$ (Fukugita & Peebles 2004). The luminosity densities are decomposed into spheroids and disk components, as

$$j_{K,tot} = j_{K,b} + j_{K,d} = b_1\,\rho_{\star,b} + d_1\,\rho_{\star,d}, \tag{B1}$$

$$j_{B,tot} = j_{B,b} + j_{B,d} = b_2\,\rho_{\star,b} + d_2\,\rho_{\star,d} \tag{B2}$$

where the subscripts b and d stand for the spheroid and the disk, with the coefficients the inverse of the stellar mass-to-light ratios $b_1 = (L_K/M_\star)_b$, $b_2 = (L_B/M_\star)_b$, $d_1 = (L_K/M_\star)_d$, and $d_2 = (L_B/M_\star)_d$. The BClib03 model give $b_1 = (0.86)^{-1} = 1.16$, $b_2 = (5.59)^{-1} = 0.18$, $d_1 = (0.55)^{-1} = 1.82$, and $d_2 = (1.20)^{-1} = 0.83$. We solve the equations and obtain $\rho_{\star,b} = 1.63 \times 10^8\, M_\odot\ \mathrm{Mpc}^{-3}$ and $\rho_{\star,d} = 1.21 \times 10^8\, M_\odot\ \mathrm{Mpc}^{-3}$. The corresponding stellar mass density parameters are $\Omega_\star = 0.00120$ (bulge) and 0.00089 (disk) as presented in Table 2 and 3, which means the mean bulge-to-disk mass ratio $(M_b/M_d) = 1.35$ (or equivalently $M_b : M_d = 57\% : 43\%$). This bulge mass fraction is somewhat smaller than the one obtained by explicit summation over the galaxy sample, but it is within the expected uncertainty of $\sim 20\%$. We note that this method does not work well if one uses the r-band luminosity instead of B-band luminosity, because r-band is not sensitive enough to young stars that dominate the disk component.

REFERENCES

Abadi, M. G., Navarro, J. F., Steinmetz, M., & Eke, V. R. 2003, ApJ, 591, 499

Aharonian, F., Akhperjanian, A. G., Bazer-Bachi, A. R., Beilicke, M., Benbow, W., Berge, D., Bernlöhr, K., Boisson, C., et al. 2006, Nature, 440, 1018

Arnett, D. 1996, Supernovae and nucleosynthesis. an investigation of the history of matter, from the Big Bang to the present (Princeton series in astrophysics, Princeton, NJ: Princeton University Press, 1996)

Ascasibar, Y., Yepes, G., Gottlöber, S., & Müller, V. 2002, A&A, 387, 396

Baade, W. 1944, ApJ, 100, 137

Baldry, I. K., Glazebrook, K., Brinkmann, J., Ivezic, Z., Lupton, R. H., Nichol, R. C., & Szalay, A. S. 2004, ApJ, 600, 681

Balogh, M. L., Baldry, I. K., Nichol, R., Miller, C., Bower, R., & Glazebrook, K. 2004, ApJ, 615, L101

Barger, A. J., Cowie, L. L., & Richards, E. A. 2000, AJ, 119, 2092

Bell, E. F., McIntosh, D. H., Katz, N., & Weinberg, M. D. 2003, ApJ, 149, 289

Bernardi, M., Sheth, R. K., Annis, J., Burles, S., Eisenstein, D. J., Finkbeiner, D. P., Hogg, D. W., Lupton, R. H., et al. 2003, AJ, 125, 1866

Bernstein, R. A., Freedman, W. L., & Madore, B. F. 2002, ApJ, 571, 56

Blanton, M. R., Hogg, D. W., Bahcall, N. A., et al. 2003a, ApJ, 592, 819

Blanton, M. R. et al. 2003b, ApJ, 594, 186

Bond, J. R., Cole, S., Efstathiou, G., & Kaiser, N. 1991, ApJ, 379, 440

Bouché, N., Lehnert, M. D., & Péroux, C. 2006, MNRAS, 367, L16

Bouwens, R. J., Illingworth, G. D., Blakeslee, J. P., & Franx, M. 2005, ApJ, accepted (astro-ph/0509641)

Bouwens, R. J., Illingworth, G. D., Thompson, R. I., Blakeslee, J. P., Dickinson, M. E., Broadhurst, T. J., Eisenstein, D. J., Fan, X., et al. 2004, ApJ, 606, L25

Brinchmann, J., Charlot, S., White, S. D. M., Tremonti, C., Kauffmann, G., Heckman, T., & Brinkmann, J. 2004, MNRAS, 351, 1151

Brinchmann, J. & Ellis, R. 2000, ApJ, 536, L77

Bruzual, G. & Charlot, S. 2003, MNRAS, 344, 1000

Bunker, A. J., Stanway, E. R., Ellis, R. S., & McMahon, R. G. 2004, MNRAS, 355, 374

Cambresy, L., Reach, W. T., Beichman, C. A., & Jarrett, T. H. 2001, ApJ, 555, 563

Cen, R., Nagamine, K., & Ostriker, J. P. 2005, ApJ, 635, 86

Cen, R. & Ostriker, J. P. 1993, ApJ, 417, 404

Chabrier, G. 2003, ApJ, 586, L133

Cimatti, A., Daddi, E., Renzini, A., Cassata, P., Vanzella, E., Pozzetti, L., Cristiani, S., Fontana, A., et al. 2004, Nature, 430, 184

Cole, S., Lacey, C. G., Baugh, C. M., & Frenk, C. S. 2000, MNRAS, 319, 168

Cole, S., Norberg, P., Baugh, C. M., Frenk, C. S., Bland-Hawthorn, J., Bridges, T., Cannon, R., Colless, M., Collins, C., et al. 2001, MNRAS, 326, 255

Cooray, A., Bock, J. J., Keatin, B., Lange, A. E., & Matsumoto, T. 2004, ApJ, 606, 611

Cowie, L. L., Songaila, A., & Barger, A. J. 1999, AJ, 118, 603

Dickinson, M., Stern, D., Giavalisco, M., Ferguson, H. C., Tsvetanov, Z., Chornock, R., Cristiani, S., Dawson, S., et al. 2003, ApJ, 600, L99

Dole, H., Lagache, G., Puget, J.-L., Caputi, K. I., Fernández-Conde, N., Le Floc'h, E., Papovich, C., Pérez-González, P. G., et al. 2006, A&A, 451, 417

Dunne, L., Eales, S. A., & Edmunds, M. G. 2003, MNRAS, 341, 589

Dwek, E., Arendt, R. G., & Krennrich, F. 2005a, ApJ, 635, 784

Dwek, E., Krennrich, F., & Arendt, R. G. 2005b, ApJ, 634, 155

Faber, S. M. & Jackson, R. E. 1976, ApJ, 204, 668

Fernandez, E. & Komatsu, E. 2005, astro-ph/0508174

Fontana, A., Pozzetti, L., Donnarumma, I., Renzini, A., Cimatti, A., Zamorani, G., Menci, N., Daddi, E., et al. 2004, A&A, 424, 23

Freeman, K. & Bland-Hawthorn, J. 2002, ARA&A, 40, 487

Fukugita, M., Hogan, C. J., & Peebles, P. J. E. 1996, Nature, 381, 489

Fukugita, M. & Peebles, P. J. E. 2004, ApJ, 616, 643

Gabasch, A., Salvato, M., Saglia, R. P., Bender, R., et al. 2004, ApJ, 616, L83

Gallego, J., Zamorano, J., Aragon-Salamanca, A., & Rego, M. 1995, ApJ, 459, L43

Giavalisco, M., Dickinson, M., Ferguson, H. C., Ravindranath, S., Kretchmer, C., Moustakas, L. A., Madau, P., Fall, M., et al. 2004, ApJ, 600, L103

Glazebrook, K., Abraham, R., McCarthy, P., Savaglio, S., Chen, H.-W., Crampton, D., Murowinski, R., Jorgensen, I., et al. 2004, Nature, 430, 181

Hauser, M. G. & Dwek, E. 2001, ARA&A, 39, 249

Heavens, A. F., Jimenez, R., & Lahav, O. 2000, MNRAS, 317, 965

Heavens, A. F., Panter, B., Jimenez, R., & Dunlop, J. 2004, Nature, 428, 625

Hernquist, L. & Springel, V. 2003, MNRAS, 341, 1253

Hopkins, A. M. 2004, ApJ, 615, 209

Hopkins, A. M., Connolly, A. J., & Szalay, A. S. 2000, AJ, 120, 2843

Iwata, I., Ohta, K., Tamura, N., Ando, M., Wada, S., Watanabe, C., Akiyama, M., & Aoki, K. 2003, PASJ, 55, 415

Kashlinsky, A. 2005, Phys. Rep., 409, 361

Kashlinsky, A., Arendt, R., Gardner, J. P., Mather, J. C., & Moseley, S. H. 2004, ApJ, 608, 1

Kauffmann, G., White, S. D. M., & Guiderdoni, B. 1993, MNRAS, 264, 201

Kauffmann, G. et al. 2003, MNRAS, 341, 54

Kneiske, T. M., Mannheim, K., & Hartmann, D. H. 2002, A&A, 386, 1

Kochanek, C. S., Pahre, M. A., Falco, E. E., Huchra, J. P., et al. 2001, ApJ, 560, 566

Lacey, C. & Cole, S. 1993, MNRAS, 262, 627

Lanzetta, K. M., Yahata, N., Pascarelle, S., Chen, H.-W., & Fernández-Soto, A. 2002, ApJ, 570, 492

Lilly, S. J., Fèvre, O. L., Hammer, F., & Crampton, D. 1996, ApJ, 460, L1

Madau, P., Ferguson, H. C., Dickinson, E. D., Giavalisco, M., Steidel, C. C., & Fruchter, A. 1996, MNRAS, 283, 1388

Madau, P. & Pozzetti, L. 2000, MNRAS, 312, L9

Madau, P., Pozzetti, L., & Dickinson, M. 1998, ApJ, 498, 106

Madau, P. & Silk, J. 2005, MNRAS, 359, L37

Matsumoto, M. 2001, in "The extragalactic infrared background and its cosmological implications", IAU Symposium 204, ed. M. Harwit & M. G. Hauser, 101

Matsumoto, T., Matsuura, S., Murakami, H., Tanaka, M., et al. 2005, ApJ, 626, 31

Mattila, K. 2003, ApJ, 591, 119

McCarthy, P. J. 2004, ARA&A, 42, 477

McCarthy, P. J., Le Borgne, D., Crampton, D., Chen, H.-W., Abraham, R. G., Glazebrook, K., Savaglio, S., Carlberg, R. G., et al. 2004, ApJ, 614, L9

Naab, T., Johansson, P. H., Efstathiou, G., & Ostriker, J. P. 2005, astro-ph/0512235

Naab, T. & Ostriker, J. P. 2006, MNRAS, 366, 899

Nagamine, K., Cen, R., Furlanetto, S. R., Hernquist, L., Night, C., Ostriker, J. P., & Ouchi, M. 2006, New Astronomy Review, 50, 29

Nagamine, K., Cen, R., Hernquist, L., Ostriker, J. P., & Springel, V. 2004, ApJ, 610, 45

—. 2005a, ApJ, 627, 608

—. 2005b, ApJ, 618, 23

Nagamine, K., Cen, R., & Ostriker, J. P. 2000, ApJ, 541, 25

Nagamine, K., Fukugita, M., Cen, R., & Ostriker, J. P. 2001a, MNRAS, 327, L10

—. 2001b, ApJ, 558, 497

Nakamura, O., Fukugita, M., Brinkmann, J., & Schneider, D. P. 2004, AJ, 127, 2511

Nakamura, O., Fukugita, M., Yasuda, N., Loveday, J., Brinkmann, J., Schneider, D. P., Shimasaku, K., & SubbaRao, M. 2003, AJ, 125, 1682

Nelan, J. E., Smith, R. J., Hudson, M. J., Wegner, G. A., Lucey, J. R., Moore, S. A. W., Quinney, S. J., & Suntzeff, N. B. 2005, ApJ, 632, 137

Norman, C., Ptak, A., Hornschemeier, A., Hasinger, G., Bergeron, J., Comastri, A., Giacconi, R., Gilli, R., et al. 2004, ApJ, 607, 721

Ohama, N. 2003, PhD thesis, University of Tokyo

Oort, J. H. 1926, PGro, 40, 1

Ostriker, J. P. & Steinhardt, P. J. 1995, Nature, 377, 600

Ouchi, M., Shimasaku, K., Furusawa, H., Miyazaki, M., Doi, M., Hamabe, M., Hayashino, T., Kimura, M., et al. 2004a, ApJ, 611, 660

Panter, B., Heavens, A. F., & Jimenez, R. 2004, MNRAS, 355, 764

Pascual, S., Gallego, J., Aragón-Salamanca, A., & Zamorano, J. 2001, A&A, 379, 798

Perlmutter, S. et al. 1998, Nature, 391, 51

Prochaska, J. X., O'Meara, J. M., Herbert-Fort, S., Burles, S., Prochter, G. E., & Bernstein, R. A. 2006, submitted, astro-ph/0606573

Reddy, N. A., Erb, D. K., Steidel, C. C., Shapley, A. E., Adelberger, K. L., & Pettini, M. 2005, ApJ, 633, 748

Reddy, N. A. & Steidel, C. C. 2004, ApJ, 603, L13

Ricotti, M. & Ostriker, J. P. 2004, MNRAS, 350, 539

Riess, A. G. et al. 1998, AJ, 116, 1009

Robin, A. C., Reylé, C., Derriére, S., & Picaud, S. 2003, A&A, 409, 523

Rocha-Pinto, H. J., Scalo, J., Maciel, W. J., & Flynn, C. 2000, A&A, 358, 869

Rudnick, G., Rix, H.-W., Franx, M., Labbe, I., Blanton, M., Daddi, E., Förster, S., Natascha, M., et al. 2003, ApJ, 599, 847

Sakai, S., Mould, J. R., Hughes, S. M. G., Huchra, J. P., et al. 2000, ApJ, 529, 698

Salvaterra, R. & Ferrara, A. 2003, MNRAS, 339, 973

Searle, L., Sargent, W. L. W., & Bagnuolo, W. G. 1973, ApJ, 179, 427

Somerville, R. S., Moustakas, L. A., Mobasher, B., Gardner, J. P., Cimatti, A., Conselice, C., Daddi, E., Dahlen, T., et al. 2004, ApJ, 600, L135

Somerville, R. S., Primack, J. R., & Faber, S. M. 2001, MNRAS, 320, 504

Spergel, D., Verde, L., Peiris, H. V., Komatsu, E., Nolta, M. R., Bennett, C. L., Halpern, M., Hinshaw, G., et al. 2003, ApJS, 148, 175

Springel, V. & Hernquist, L. 2003a, MNRAS, 339, 289

—. 2003b, MNRAS, 339, 312

Steidel, C. C., Adelberger, K. L., Giavalisco, M., Dickinson, M., & Pettini, M. 1999, ApJ, 519, 1

Strateva, I. et al. 2001, AJ, 122, 1861

Tegmark, M., Strauss, M. A., Blanton, M. R., et al. 2004, PhRvD, 69, 13501

Thompson, R. I. 2003, ApJ, 596, 748

Thompson, R. I., Eisenstein, D., Fan, X., Dickinson, M., Illingworth, G., & Kennicutt, R. C. 2006, astro-ph/0605060

Totani, T., Yoshii, Y., Iwamuro, F., Maihara, T., & Motohara, K. 2001, ApJ, 550, L137

Tresse, L. & Maddox, S. J. 1998, ApJ, 495, 691

Tresse, L., Maddox, S. J., Févre, O. L., & Cuby, J.-G. 2002, MNRAS, 337, 369

Tully, B., Pierce, M. J., J.-S. Huang, W. S., Verheijen, M. A. W., & Witchalls, P. L. 1998, AJ, 115, 2264

Vale, A. & Ostriker, J. P. 2004, MNRAS, 353, 189

Williams, R. E. et al. 1996, AJ, 112, 1335

York, D. G. et al. 2000, AJ, 120, 1579

Table 1. Bulge-disk luminosity decomposition based on SDSS data

	E	S0	S0/a-Sb	Sbc-Sd	Irr	j_r
j_r [a]	0.21	0.41	1.00	0.37	0.02	2.00
B/T [b]	1.00	0.62	0.40	0.24	0.00	0.95
D/T [c]	0.00	0.38	0.60	0.76	1.00	1.05

[a] r band luminosity density contributed by each Hubble type of galaxies from Nakamura et al. (2003).

[b,c] Bulge-to-total and disk-to-total luminosity ratios for each type of galaxies from Ohama (2003).

Note. — The last column gives the r band luminosity densities for the bulge and disc components in units of $10^8\,hL_{\odot,r}\,\mathrm{Mpc}^{-3}$, which yield $j_r(B)/j_r(D) = 0.91$. Extinction corrections are applied to the disk component, using $A_R = \gamma_R \log(a/b)$, where a/b is the axis ratio, and $\gamma_R = 1.15 + 1.88(\log W_{20\%} - 2.5) = 1.24$ at $\log W_{20\%} = 2.55$ for $R^* = -21.09$ from Sakai et al. (2000, see also Tully et al. (1998)): for $\log\langle a/b\rangle = 0.22$ we obtain $\langle A_R\rangle = 0.27$, where the difference between R and r is ignored. This leads us to the corrected bulge-to-disk ratio for the luminosity density, $j_r(B)/j_r(D)|_{\rm corr} = j_r(B)/j_r(D)10^{0.4\langle A_R\rangle} = 0.71$. We assign a 20% error to this quantity.

Table 2. Properties of the Fossil model at $z = 0$

Population	$\Omega_\star$	τ [a]	$Z/Z_\odot$ [b]	$\langle t_{\rm age}\rangle$ [c]	$u-g$	$g-r$	$(M_\star/L_B)$ [d]	$(M_\star/L_r)$ [e]	$(M_\star/L_K)$ [f]
Bulge	0.00120	1.5	1.5	10.5	1.78	0.84	5.59	3.19	0.86
Disk	0.00089	4.5	0.8	7.0	0.94	0.43	1.20	1.18	0.55

[a] Characteristic time-scale in units of Gyr [defined in Equation (1)].

[b] Metallicity ($Z_\odot = 0.02$).

[c] Mean age of stars in units of Gyr.

[d−f] Stellar-mass-to-light ratio in solar units for the B, r, K-bands and the Chabrier IMF ($0.01 - 100\,M_\odot$). Stellar masses include the remnants.

Table 3. Physical quantities at $z = 0$ for the models used in the text

Model	$\Omega_\star$ [†]	$M_\star$ [♮]	$M_{\rm rem}$ [∀]	I_{EBL} [‡]	$\dot{\rho}_\star$ [§]	$j_{\rm bol}$ [a]	j_U [b]	j_B [c]	j_r [d]	j_K [e]	$u-g$	$g-r$
Fossil	0.0021	2.26	0.58	42	0.86	3.0	1.4	1.3	1.5	4.1	1.54	0.67
..... bulge	0.00120	1.28	0.36	22	0.022	0.9	0.2	0.3	0.5	1.9	1.78	0.84
..... disk	0.00089	0.99	0.22	20	0.837	2.1	1.2	1.0	1.0	2.2	0.94	0.43
TVD	0.0028	3.06	0.80	51	1.02	3.2	1.5	1.4	1.8	5.1	1.20	0.61
H&S	0.0021	2.23	0.56	37	1.30	3.2	1.7	1.5	1.6	4.1	1.00	0.50
SA	0.0023	2.56	0.61	47	1.37	3.7	2.0	1.7	2.0	4.9	1.04	0.52
Consensus	0.0023	2.52	0.65	43	1.06	3.1	1.5	1.4	1.6	4.4	1.25	0.59
Model[¶]	±0.0004	±0.47	±0.13	±7	±0.22	±0.2	±0.2	±0.1	±0.2	±0.6	±0.27	±0.09
Observed	0.0018	—	—	42–	0.5	3.2	1.4	1.2	1.27	3.4	—	—
range	−0.0039	—	—	135	−1.6	−5.0	−1.8	−2.0	−1.33	−5.5	—	—

[†] Stellar mass density including the remnants for Chabrier IMF ($0.01 - 100\,M_\odot$).

[♮] Stellar mass density without the remnants (in $10^8\,M_\odot$ Mpc^{-3}).

[∀] Stellar remnant mass density (in $10^8\,M_\odot$ Mpc^{-3}).

[‡] EBL intensity (in nW m^{-2} sr^{-1}).

[§] SFR density (in $10^{-2}\,M_\odot\,{\rm yr}^{-1}$ Mpc^{-3}).

[a] Bolometric luminosity density (in $10^8\,L_{\odot,{\rm bol}}\,{\rm Mpc}^{-3}$).

[b–e] Luminosity density in U, B, r, K-bands (in $10^8\,L_{\odot,B}\,{\rm Mpc}^{-3}$).

[¶] Average of the Fossil, TVD, and H&S models, with errors being the dispersion among the three models.

Note. — Bolometric magnitudes $M_{B,\odot} = 5.48$, $M_{K,\odot} = 3.28$ and $M_{r,\odot} = 4.76$ are adopted for the Sun. Model luminosity densities are compared with observations: $j_B = (1.7 \pm 0.3) \times 10^8\,L_{\odot,B}\,{\rm Mpc}^{-3}$ (Nagamine et al. 2001a), $j_B = (1.3 \pm 0.1) \times 10^8\,L_{\odot,B}\,{\rm Mpc}^{-3}$ (Fukugita & Peebles 2004), $j_r = (1.3 \pm 0.03) \times 10^8\,L_{\odot,r}\,{\rm Mpc}^{-3}$ (at $z = 0.1$, Blanton et al. 2003a), $j_K = 4.1^{+2.0}_{-0.6} \times 10^8\,L_{\odot,K}\,{\rm Mpc}^{-3}$ (Bell et al. 2003), $(5.0 \pm 0.5) \times 10^8\,L_{\odot,K}\,{\rm Mpc}^{-3}$ (Kochanek et al. 2001), $j_{Ks} = (4.0 \pm 0.6) \times 10^8\,L_{\odot,Ks}\,{\rm Mpc}^{-3}$ (Cole et al. 2001). All values assume $h = 0.7$.

Table 4. Mean metallicity of spheroids

Type	$\langle Z/Z_\odot \rangle$ [a]	$j_r\,[10^8\,h\,L_{r,\odot}\,\mathrm{Mpc}^{-3}]$ [b]
E-S0	1.44	0.70
S0/a–Sb	1.15	0.39
Sbc–Sd	1.15	0.082
Total	1.33	1.17

[a] Mass weighted mean metallicity.

[b] r-band luminosity density from the spheroid component.

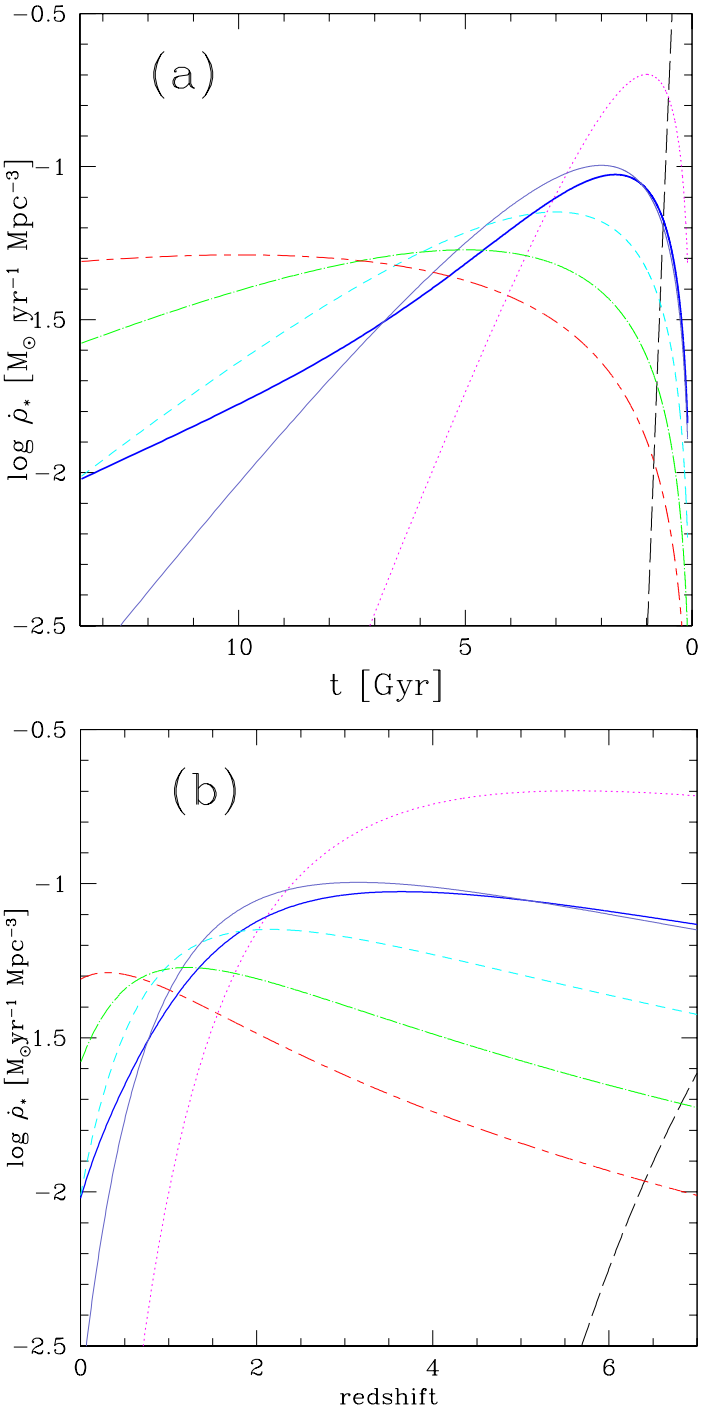

Fig. 1.— Star formation histories of delayed exponential decay model as functions of cosmic time (*panel a*) and redshift (*panel b*). The normalization is fixed to equation (2) for each model. The lines are for $\tau = 0.1$ Gyr (black long-dashed), 1 Gyr (magenta dotted), 2 Gyr (blue solid), 3 Gyr (cyan dashed), 5 Gyr (green dot-dashed), and 10 Gyrs (red long-short-dashed). The blue thick solid line is the composite two population model with $\tau = 1.5$ Gyr and 4.5 Gyr, which is taken as our 'Fossil' model.

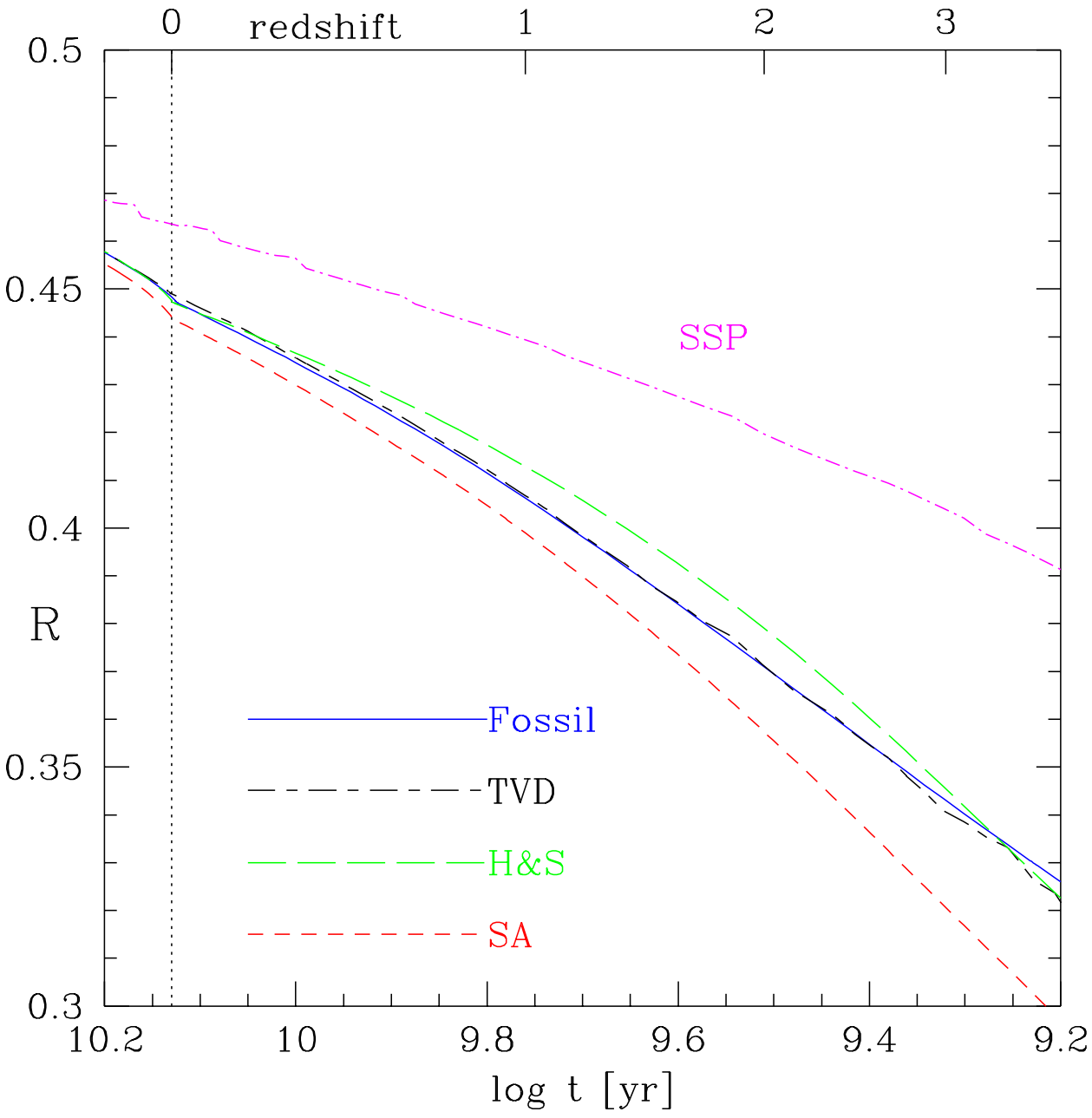

Fig. 2.— Gas recycling fraction R as a function of cosmic time (and redshift), computed using BClib03 for solar metallicity and the Chabrier IMF ($0.01 - 100\,M_{\odot}$). 'SSP' stands for 'Simple Stellar Population' with an instantaneous burst at $t = 0$.

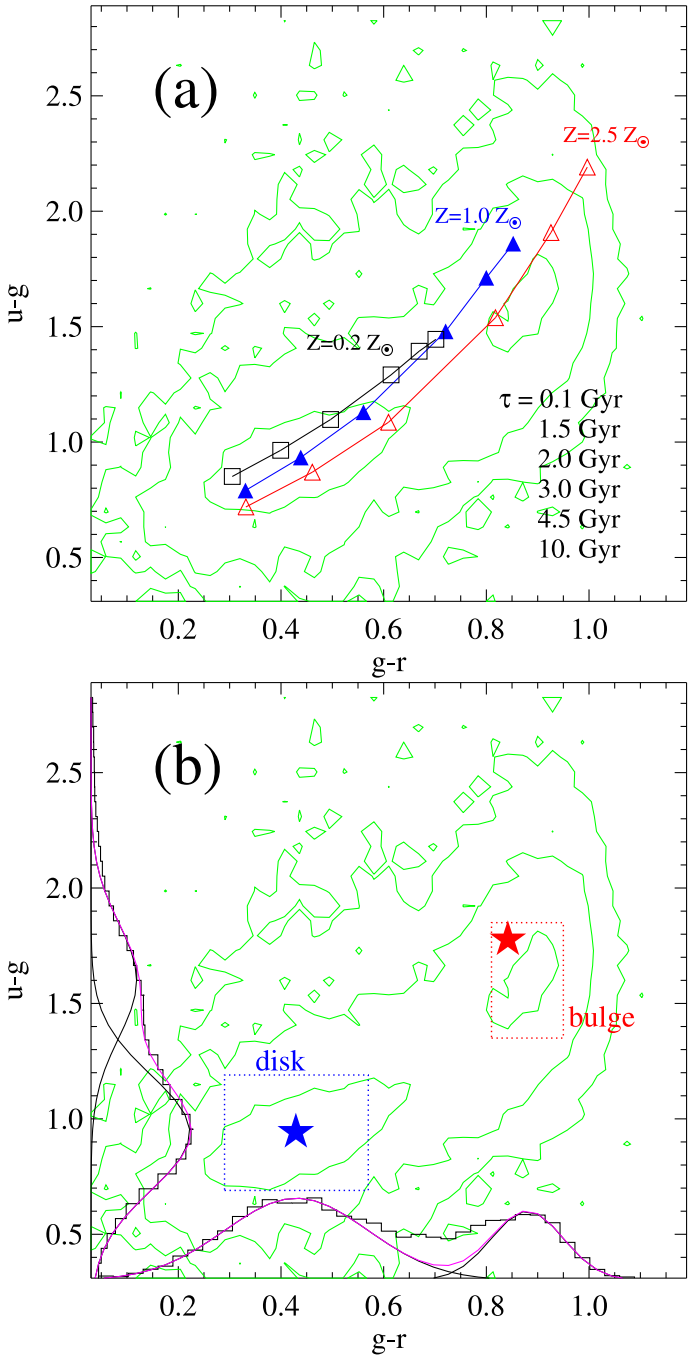

Fig. 3.— *Panel (a):* Color-color diagram in $u-g$ vs. $g-r$ plane. The three lines represent the delayed exponential decay models with Chabrier IMF for metallicities: $Z/Z_{\odot} = 0.2$ (*black open squares*), 1.0 (*blue solid triangles*), and 2.5 (*red open triangles*), with τ running along the line from top to bottom as indicated in the legend. The contour shows the color distribution for SDSS galaxies taken from Blanton et al. (2003b). *Panel (b):* Same as (a), but with the histogram for the color distribution of SDSS galaxies projected onto the axes together with Gaussian fits. The two boxes indicate the location of the peaks of the histogram, with the widths twice the dispersions of the Gaussian. The asterisks indicate the bulge component (with $\tau = 1.5\,\mathrm{Gyr}$, $Z/Z_{\odot} = 1.5$) and the disk component (with $\tau = 4.5\,\mathrm{Gyr}$, $Z/Z_{\odot} = 0.8$) of the 'Fossil' model.

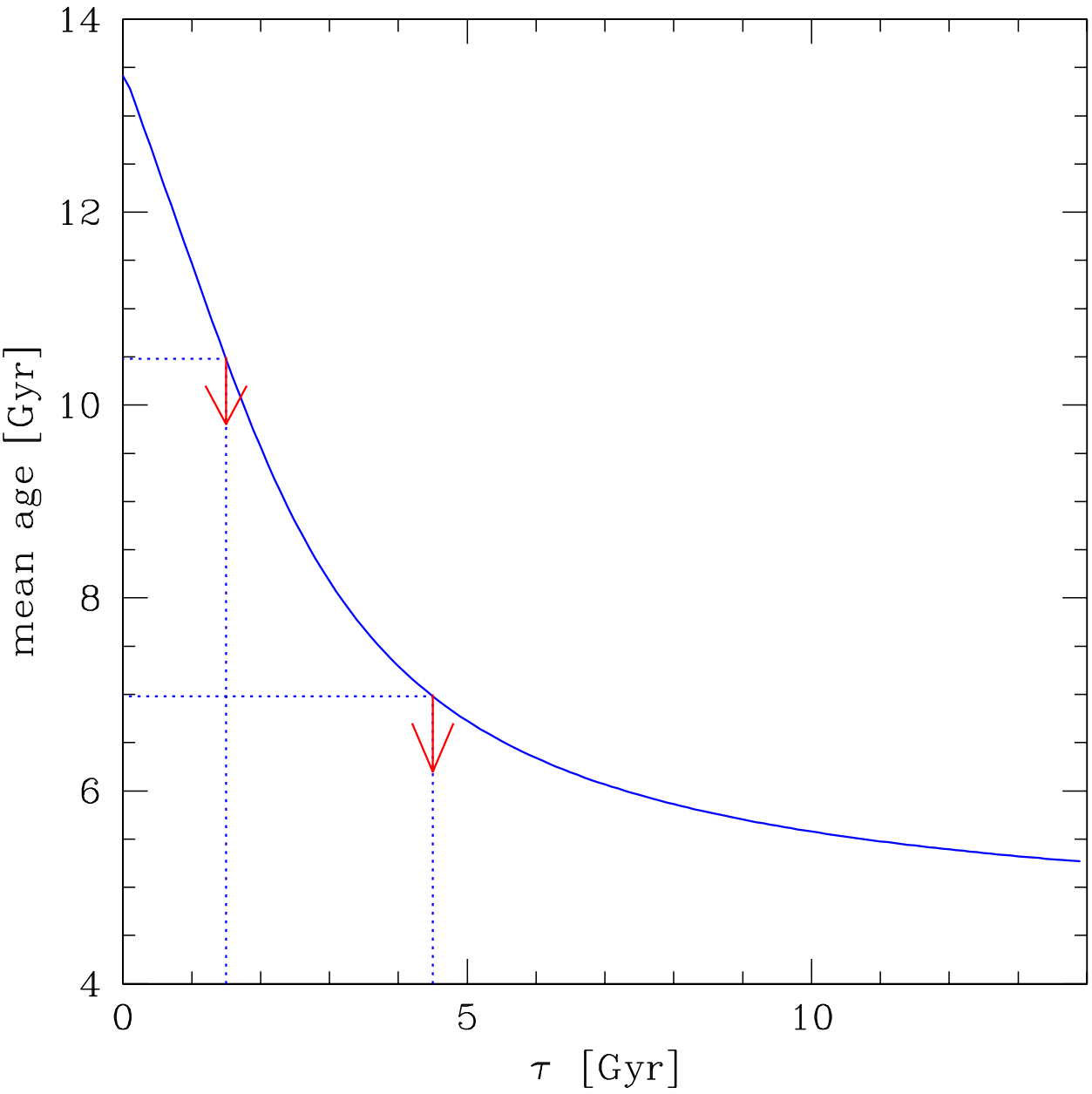

Fig. 4.— Mean age of stars as a function of decay time τ for the delayed exponential model. The dotted lines shows the values of τ ($\tau = 1.5\,\mathrm{Gyr}$ and $4.5\,\mathrm{Gyr}$) adopted for the 'Fossil' model. The arrows indicate the shift in the mean age when stellar remnants are removed from the calculation, while the curve includes the contribution from the dead stars that are not emitting light at the present time, therefore push the age up.

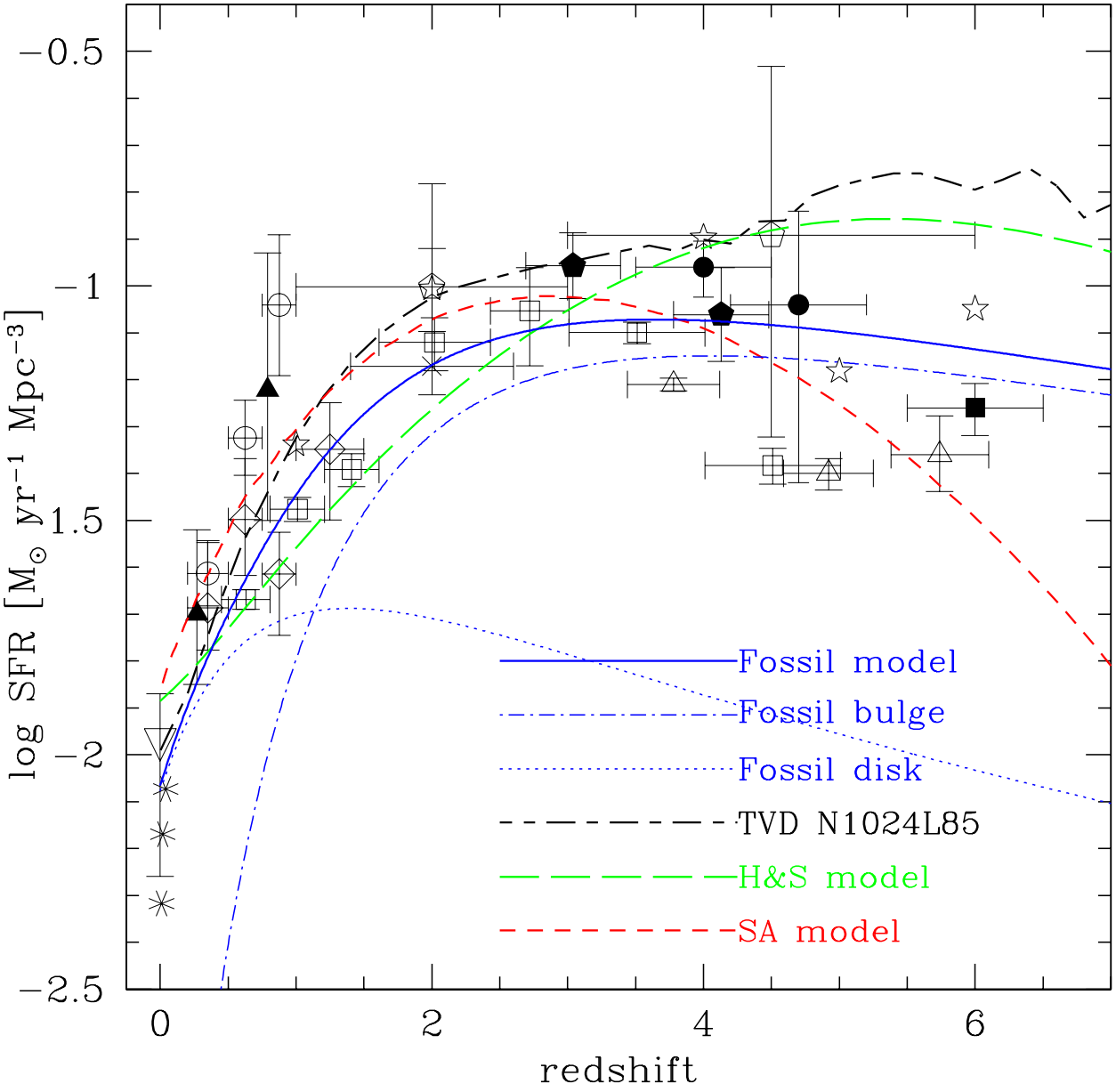

Fig. 5.— Star formation rate density as a function of redshift. The curves represent the model predictions specified in the legend. The data are taken from (from low to high redshift): Heavens et al. (2004, 3 asterisks at $z \sim 0$), Nakamura et al. (2004, open inverted triangle at $z = 0$), Lilly et al. (1996, open circles), Norman et al. (2004, filled triangles), Cowie et al. (1999, open diamonds), Gabasch et al. (2004, open squares), Reddy et al. (2005, cross at $z = 2$), Barger et al. (2000, open pentagons at $z = 2$ and 4.5), Steidel et al. (1999, filled pentagons at $z = 3, 4$), Ouchi et al. (2004a, filled circles at $z = 4, 5$), Giavalisco et al. (2004, open triangles at $z = 3 - 6$), Bouwens et al. (2005, filled square at $z = 6$), and Thompson et al. (2006, open stars without error bars). The data are converted to the values with the Chabrier IMF and common values are assumed for dust extinction for the UV data. See text for details.

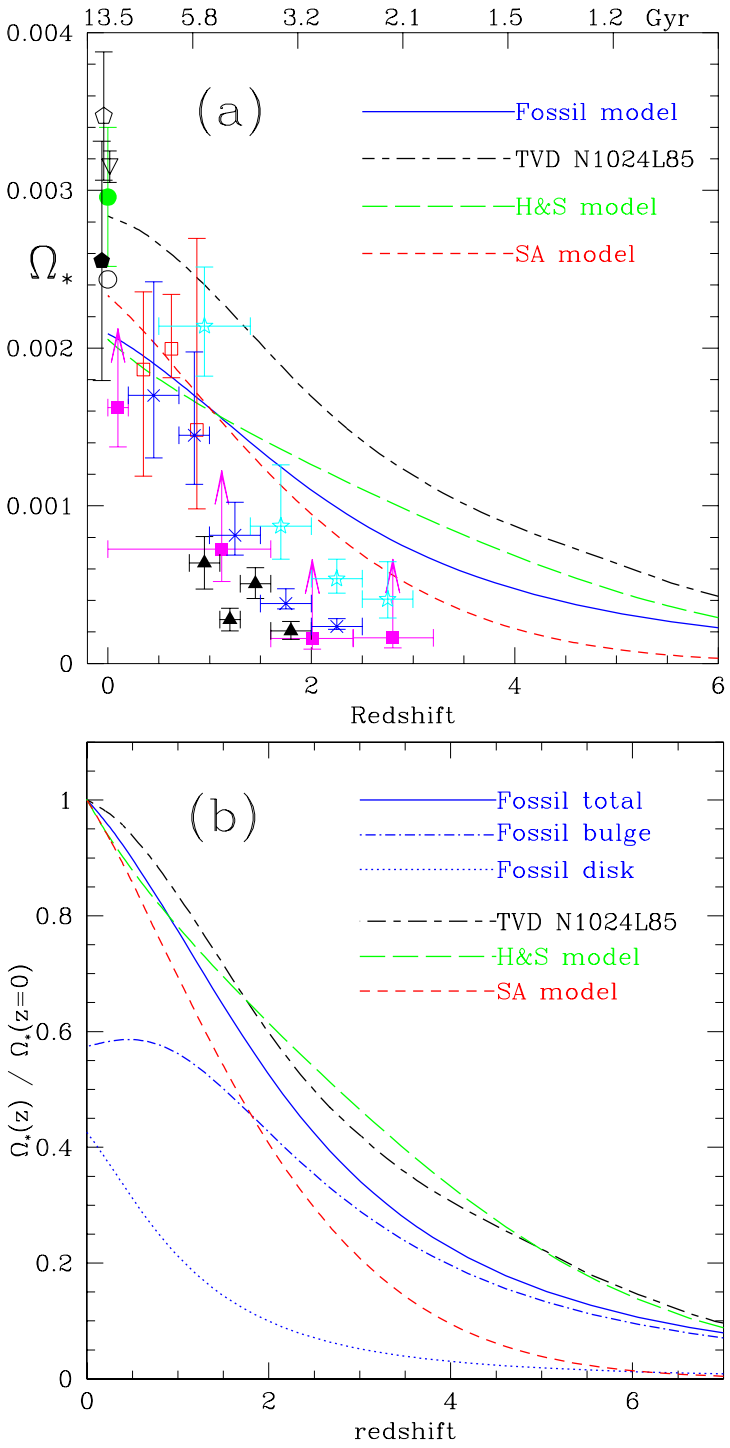

Fig. 6.— *Panel (a):* Stellar mass density (including remnants) as a function of redshift and age. The top axis indicates the age of the Universe. All data assume the Chabrier IMF and $h = 0.7$. The source of data are given in the text. *Panel (b):* Growth of the stellar mass density normalized by the value at $z = 0$. For the Fossil model, the bulge and disk components are also shown separately.

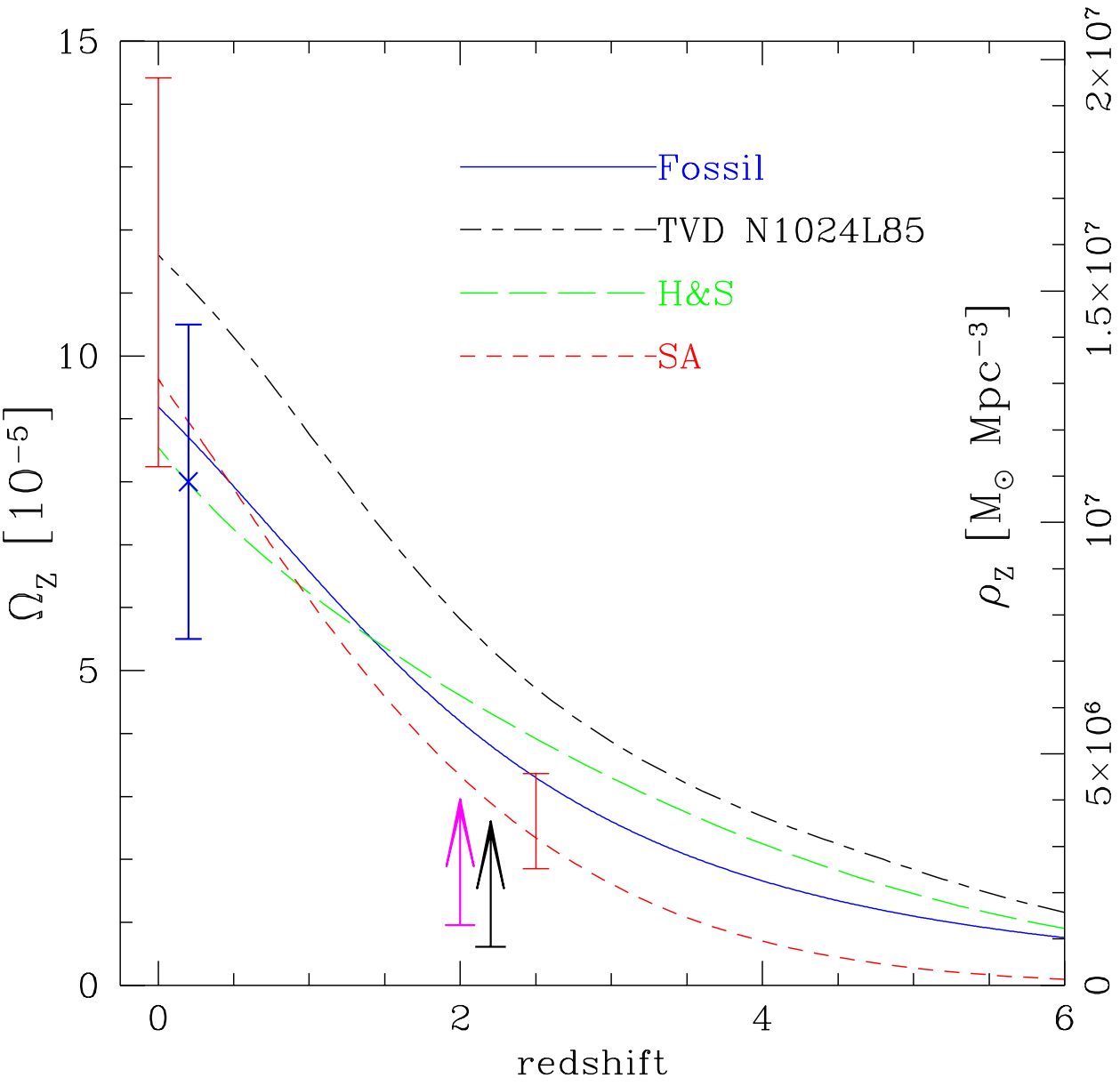

Fig. 7.— Metal mass density as a function of redshift. The curves represent the model predictions specified in the legend. The data are taken from (from low to high redshift): Dunne et al. (2003, red bars at $z = 0$ & 2.5), Fukugita & Peebles (2004, blue cross at $z = 0$, shifted for clarity), Bouché et al. (2006, magenta lower limit at $z = 2$, for galaxies), and Prochaska et al. (2006, black lower limit at $z = 2$, shifted for clarity. Only for damped Lyα systems and super Lyman Limit systems).

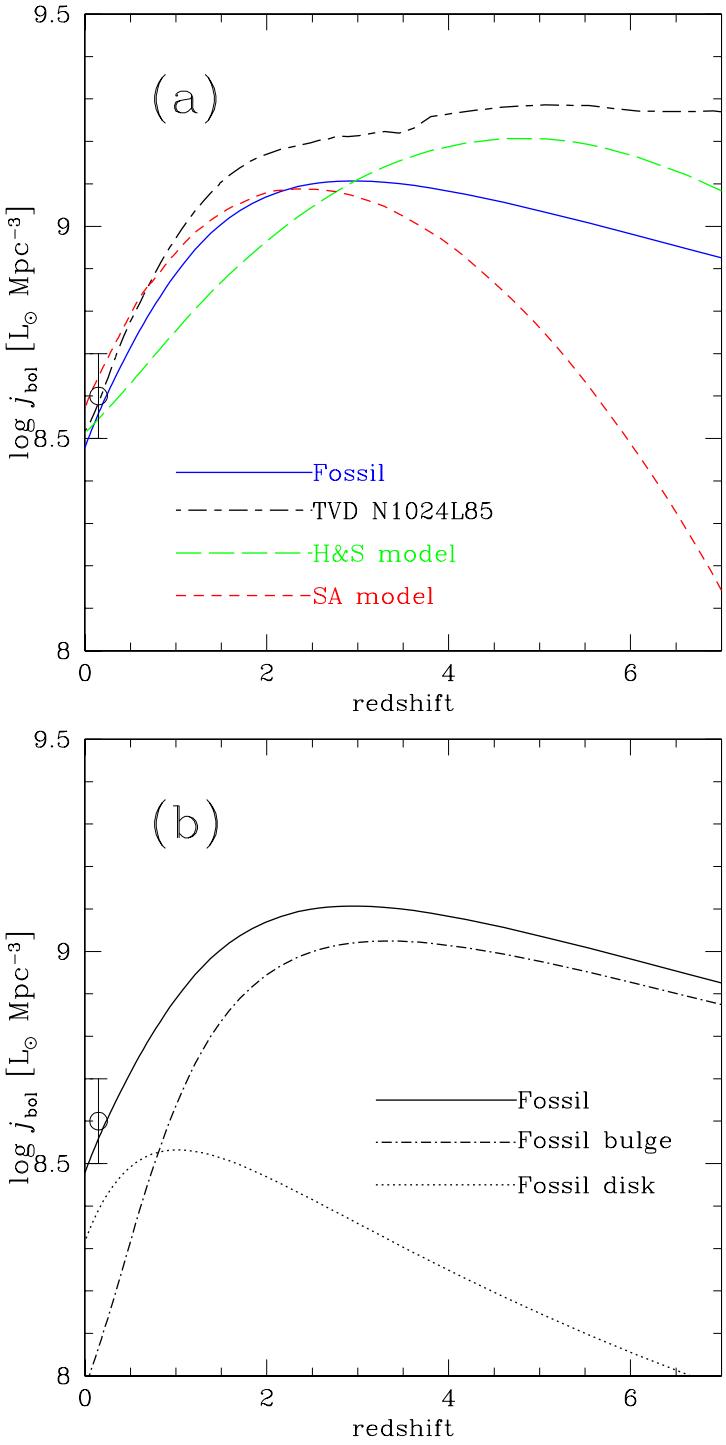

Fig. 8.— *Panel (a):* Comoving bolometric luminosity density as a function of redshift for the models indicated in the legend. *Panel (b)*: Same as (a) for the Fossil model, decomposed into the two components. The data at $z = 0$ (slightly offset to a positive z value for clarity) is the observational estimate given in Equation (14)

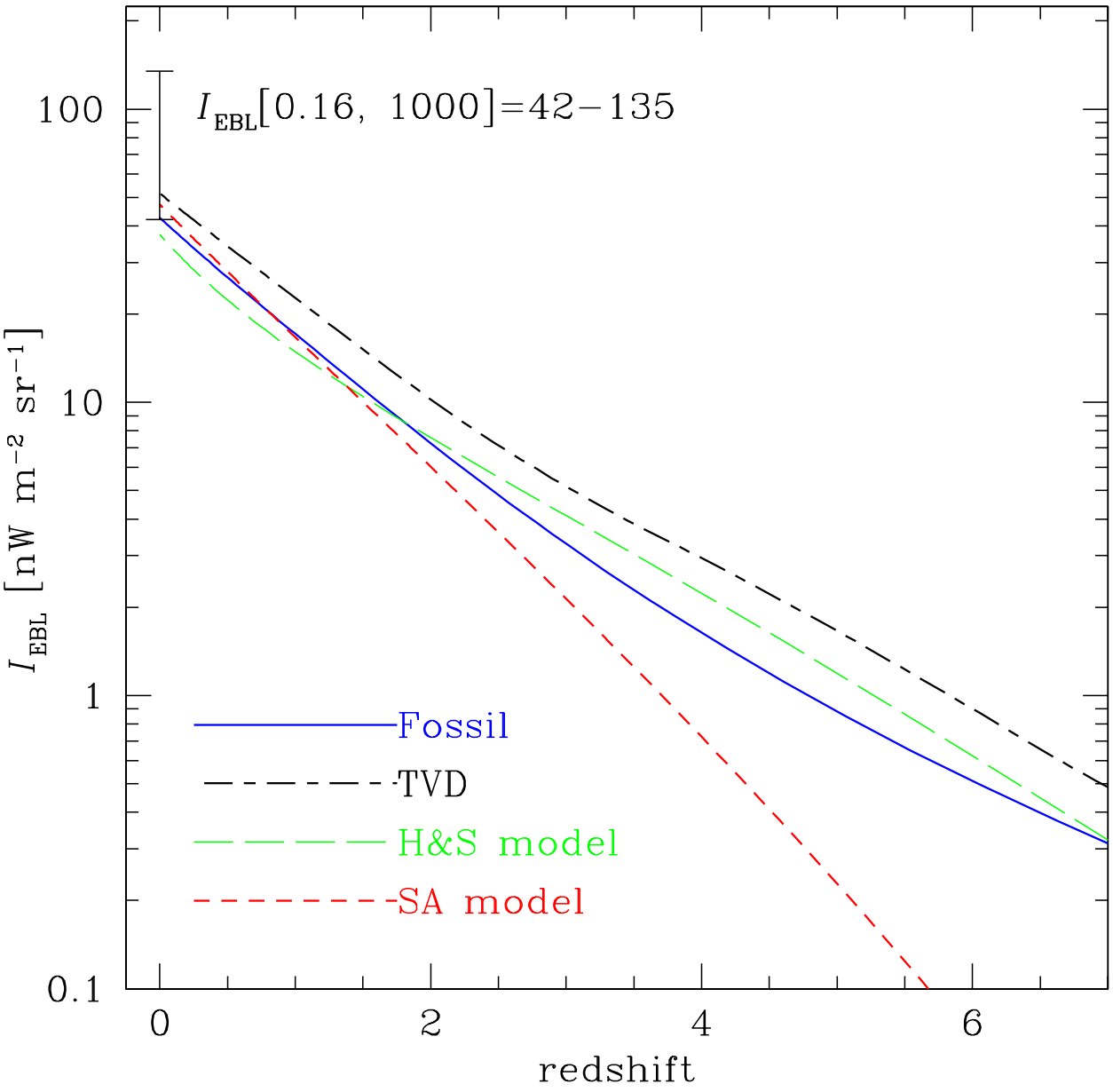

Fig. 9.— EBL as a function of redshift for the models shown in the legend. The observationally allowed range at $z = 0$, equation (9), is indicated by the error bar.

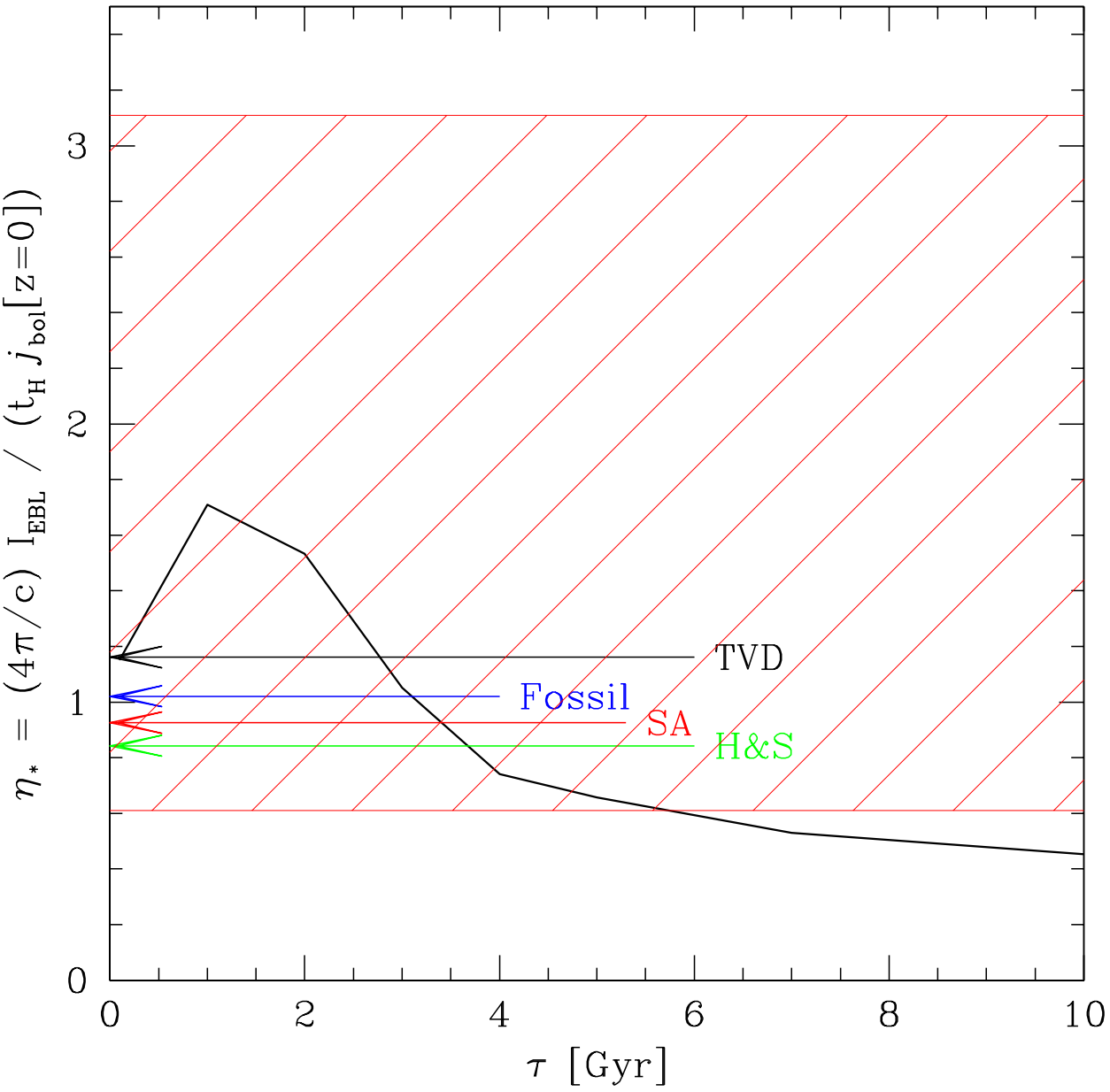

Fig. 10.— Parameter η_* of Equation (15) computed for the models used in this paper (shown by arrows). The variation of η_* is also shown as a function of decay time-scale τ for the delayed exponential model of star formation. The shaded region shows the observationally allowed range.